

Distinct regulation of autophagic activity by Atg14L and Rubicon associated with Beclin 1–phosphatidylinositol-3-kinase complex

Yun Zhong^{2,5}, Qing Jun Wang^{1,3,5}, Xianting Li¹, Ying Yan⁴, Jonathan M. Backer⁴, Brian T. Chait³, Nathaniel Heintz² and Zhenyu Yue^{1,6}

Beclin 1, a mammalian autophagy protein that has been implicated in development, tumour suppression, neurodegeneration and cell death, exists in a complex with Vps34, the class III phosphatidylinositol-3-kinase (PI(3)K) that mediates multiple vesicle-trafficking processes including endocytosis and autophagy. However, the precise role of the Beclin 1–Vps34 complex in autophagy regulation remains to be elucidated. Combining mouse genetics and biochemistry, we have identified a large *in vivo* Beclin 1 complex containing the known proteins Vps34, p150/Vps15 and UVRAG, as well as two newly identified proteins, Atg14L (yeast Atg14-like) and Rubicon (RUN domain and cysteine-rich domain containing, Beclin 1-interacting protein). Characterization of the new proteins revealed that Atg14L enhances Vps34 lipid kinase activity and upregulates autophagy, whereas Rubicon reduces Vps34 activity and downregulates autophagy. We show that Beclin 1 and Atg14L synergistically promote the formation of double-membraned organelles that are associated with Atg5 and Atg12, whereas forced expression of Rubicon results in aberrant late endosomal/lysosomal structures and impaired autophagosome maturation. We hypothesize that by forming distinct protein complexes, Beclin 1 and its binding proteins orchestrate the precise function of the class III PI(3)K in regulating autophagy at multiple steps.

Macroautophagy (herein referred to as autophagy) is a regulated process by which a portion of the cytoplasm is sequestered and delivered to lysosomes for degradation. Currently, the autophagic process in mammals is poorly understood. Identification and characterization of mammalian autophagy proteins are crucial to elucidate details of mammalian autophagy. Beclin 1 (encoded by *Becn1*, the orthologue of yeast *ATG6/Vps30*), is one of the earliest characterized mammalian autophagy proteins¹. Initially identified as a Bcl-2-binding protein², Beclin 1 has been shown both *in vitro*

and *in vivo* to participate in autophagy regulation and to have important roles in development³, tumorigenesis^{1,3–5} and neurodegeneration^{6–8}. As with yeast Atg6, Beclin 1 forms a complex with Vps34/class III PI(3)K^{9–11}. *Saccharomyces cerevisiae* has at least two Atg6/Vps34 protein complexes: one containing Atg14 and participating in autophagy, and the other containing Vps38 and functioning in non-autophagic pathways¹⁰. However, there is no concrete evidence for multiple Beclin 1–Vps34 complexes or multiple functions associated with Beclin 1–Vps34 in mammals¹¹.

To determine the mechanism by which the Beclin 1–Vps34 interaction regulates autophagy, we combined mouse genetics and biochemistry to identify Beclin 1-associated protein complexes *in vivo*. We genetically modified mice to functionally replace endogenous Beclin 1 with an enhanced green fluorescent protein-tagged Beclin 1 protein (Beclin 1–EGFP; Fig. 1a; Supplementary Information, Fig. S1a–b). In these mice (*Becn1*^{−/−}; *Becn1*–EGFP/+), only the Beclin 1–EGFP fusion protein, but not endogenous Beclin 1 was detected by an anti-Beclin 1 antibody (Fig. 1a). These mice were born at the expected Mendelian ratio (Supplementary Information, Fig. S1c), survived postnatally and were phenotypically normal at the adult stage, suggesting a full ‘rescue’ of the embryonic lethality of *Becn1*^{−/−} mice by a functional *Becn1*–EGFP transgene.

Using these ‘rescued’ mice, we isolated Beclin 1–EGFP protein complexes by affinity purification from liver, brain (Fig. 1b) and thymus (data not shown), and identified their components using mass spectrometry (Supplementary Information, Fig. S2). The rescued mice, but not the control mice, were associated with at least six readily detectable protein bands common to both liver and brain (Fig. 1b). These bands include Beclin 1–EGFP (no. 5; molecular mass of about 90,000), three previously reported Beclin 1-binding proteins p150/Vps15 (no. 1; ref. 12), Vps34 (no. 3; refs 9–11) and UVRAG (no. 4; ref. 13), and two newly identified proteins (nos 2 and 6). The first of these two proteins (no. 6, ~60K, gi|27369860) contains 492 amino acids and has a conserved SMC (structural maintenance of chromosomes) motif

¹Departments of Neurology and Neuroscience, Mount Sinai School of Medicine, New York, NY 10029, USA. ²Laboratory of Molecular Biology, Howard Hughes Medical Institute, Rockefeller University, New York, NY 10065, USA. ³Laboratory of Mass Spectrometry and Gaseous Ion Chemistry, Rockefeller University, New York, NY 10065, USA. ⁴Department of Molecular Pharmacology, Albert Einstein College of Medicine, 1300 Morris Park Avenue, Bronx, NY 10461, USA.

⁵These authors contributed equally to the work.

⁶Correspondence should be addressed to Z.Y. (e-mail: zhenyu.yue@mssm.edu)

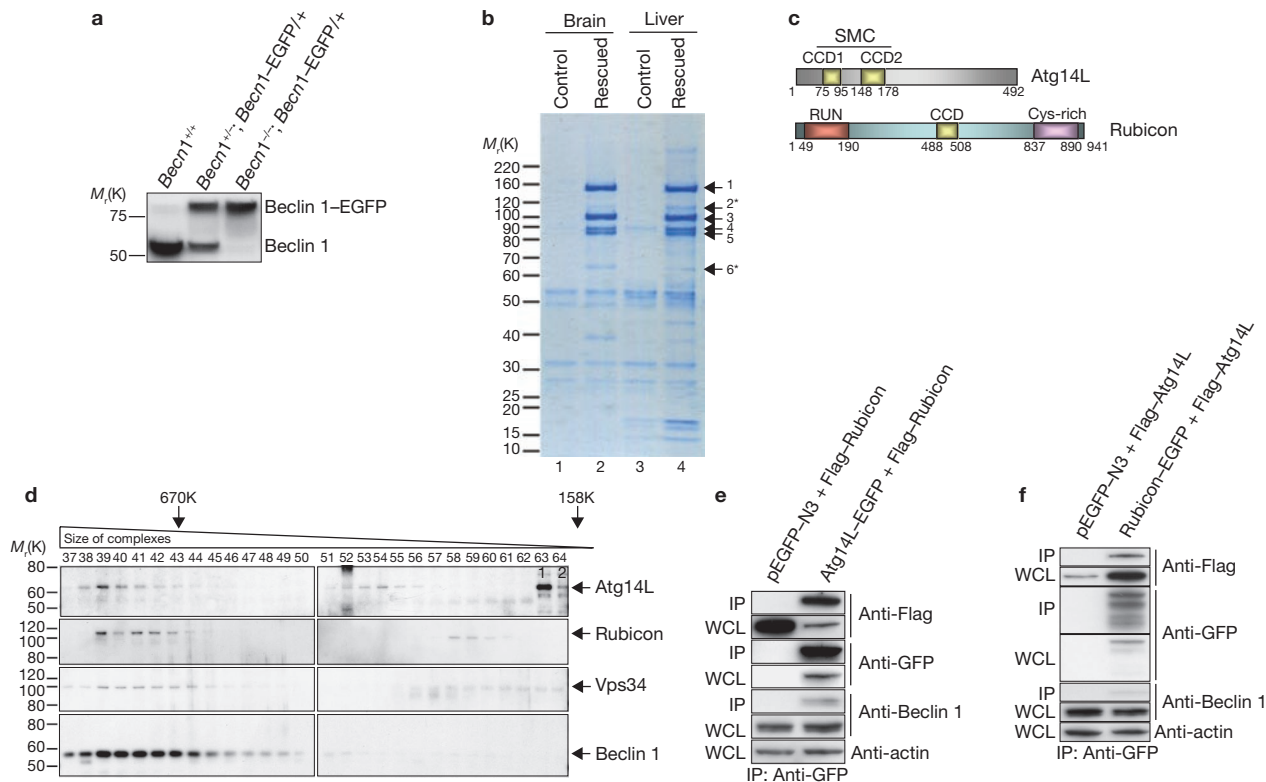


Figure 1 Identification of Beclin 1-interaction proteins from *Becn1*^{-/-};*Becn1*-EGFP/+ mice. **(a)** Western blot analysis showing the replacement of endogenous Beclin 1 with Beclin 1-EGFP in *Becn1*^{-/-};*Becn1*-EGFP/+ mice, as detected by an anti-Beclin 1 antibody. **(b)** Coomassie-stained SDS-PAGE showing the Beclin 1-interacting proteins immunoprecipitated from brain and liver of the 'rescued' mice (lanes 2 and 4) and of control *Becn1*^{-/-} littermates (lanes 1 and 3), using an anti-GFP antibody. Proteins in the gel bands were extracted and identified by mass spectrometry as Vps15/p150 (band 1), Vps34/class III PI(3)K (band 3), UVRAG (band 4), Beclin 1-EGFP (band 5), Atg14L (band 6, asterisk, gi|27369860) and Rubicon (band 2, asterisk, gi|45708948). UVRAG levels varied with different affinity-purification conditions, suggesting an unstable association of UVRAG with the complex. **(c)** Schematic representations of the domain structures of Atg14L and Rubicon. Atg14L contains two coiled-coil domains (CCD1 and CCD2), which are also homologous with the SMC domain (structural maintenance of chromosomes). Rubicon contains an N-terminal RUN (for RPIP8, UNC-14 and NESCA) domain,

or two coiled-coil domains (CCD; amino acids 75–95 and 148–178) near the amino terminus (Fig. 1c). Interestingly, the sequence of this protein shows modest similarity to yeast Atg14 (overall 15% identity; Supplementary Information, Fig. S3a). Thus, we named this protein Atg14L for yeast Atg14-like. The second protein (no. 2, ~124K, gi|45708948) contains 941 amino acids and has a conserved RUN domain (amino acids 49–190) near the amino terminus, a cysteine-rich domain (amino acids 837–890) near the carboxy terminus and a CCD (amino acids 488–508) in the central region (Fig. 1c). Thus, we named this protein Rubicon for RUN domain, a cysteine-rich domain containing, Beclin 1-interacting protein. No sequence homology was observed between Rubicon and Vps38 or Atg14 (data not shown). Notably, the protein levels of affinity-purified Beclin 1-EGFP, p150/Vps15, Vps34 and UVRAG were comparable and reproducibly higher than those of Atg14L and Rubicon (Fig. 1b), suggesting a stable 'core' Beclin 1-Vps34 complex consisting of Beclin 1, Vps34, p150 and UVRAG. Additionally, we did not detect the previously identified Beclin 1-associated proteins,

a C-terminal Cys-rich domain and a central CCD domain. **(d)** Western blot analysis of Atg14L, Rubicon, Vps34 and Beclin 1 in gel filtration fractions from wild-type mouse liver extract showed co-elution of these proteins in fractions 38–45. Atg14L was also eluted in later fractions 51–56. The fractions for the peak elution of thyroglobulin (670K) and γ -globulin (158K) are indicated by arrows. Control siRNA-transfected NIH 3T3 cell lysate was loaded as a positive control (labelled as 1) for the migration position of the Atg14L protein on SDS-PAGE; *Atg14L* siRNA-transfected NIH 3T3 cell lysate was loaded as a negative control (labelled as 2). **(e, f)** Co-immunoprecipitation confirmed protein-protein interaction between Atg14L and Rubicon. HEK 293 cells were co-transfected with Atg14L-EGFP and Flag-Rubicon **(e)** or Rubicon-EGFP and Flag-Atg14L **(f)**. Cell lysates were used for immunoprecipitation with an anti-GFP antibody and the resulting immunoprecipitates were blotted with an anti-Flag antibody. Our results show immunoprecipitation of Rubicon by Atg14L **(e)** and vice versa **(f)**. WCL, whole cell lysate; IP, immunoprecipitated. See Supplementary Information, Fig. S6 for full scans of blots in **a, d, e** and **f**.

such as nPIST⁶, Bcl-2 (ref. 2), Ambra-1 (ref. 14) or Bif1 (ref. 15), raising the possibility that their interactions with Beclin 1 may be relatively unstable, transient or occur only under specific conditions.

We next examined the specific binding of Atg14L or Rubicon to Beclin 1 in transfected mammalian cells. We showed that Flag- or EGFP-tagged Atg14L or Rubicon co-immunoprecipitated with endogenous Beclin 1 (Supplementary Information, Fig. S3b–c) and Vps34 (Supplementary Information, Fig. S3d–e). We also constructed a series of deletion mutants to analyse the sequence domains required for Beclin 1-Atg14L/Rubicon associations (Supplementary Information, Fig. S3f). We found that although the CCD of Beclin 1 is sufficient for binding Atg14L, the CCD and evolutionarily conserved domain (ECD) of Beclin 1 are necessary for binding Rubicon (Supplementary Information, Fig. S3g–h). Furthermore, both CCD domains of Atg14L are required for efficient binding of Atg14L to Beclin 1 and Vps34 (Supplementary Information, Fig. S3i), whereas the central region of Rubicon, which contains the CCD, is important for the binding of Rubicon to Beclin 1 and Vps34 (Supplementary Information,

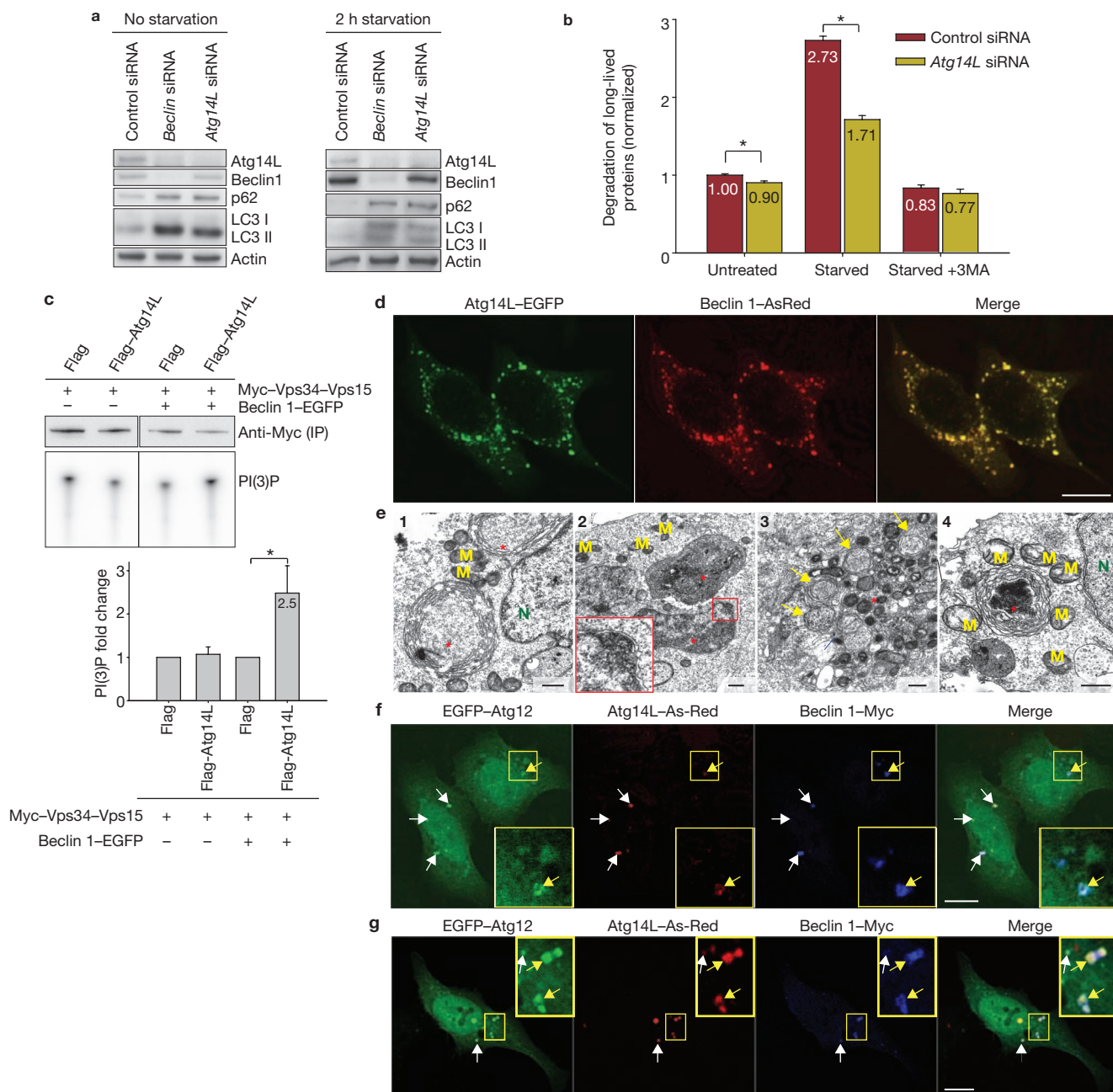


Figure 2 Atg14L positively regulates autophagy, and Beclin 1 and Atg14L synergistically promote double-membrane formation. **(a)** *Beclin 1* or *Atg14L* siRNA reduced Atg14L levels and increased p62/SQSTM1 and LC3 II levels under normal and nutrient-starvation conditions in NIH 3T3 cells. **(b)** Compared with control siRNA, *Atg14L* siRNA decreased long-lived protein degradation in NIH 3T3 cells under normal ($*P = 0.007$) and starvation ($*P = 5 \times 10^{-6}$) conditions (one-tailed Student's *t*-test with equal variances, $n = 4$). This difference was diminished when the starved cells were treated with 3-methyladenine (3MA, 10 mM), a PI(3)K inhibitor. **(c)** Vps34 kinase assay. HEK 293T cells were co-transfected with Myc-Vps34-Vps15 and Flag-Atg14L or Flag vector, either in the absence or in the presence of Beclin 1-EGFP. Myc-Vps34-Vps15 was immunoprecipitated by anti-Myc antibody for the *in vitro* kinase assay. The resulting radioactive PI(3)P was separated by thin-layer chromatography (TLC), quantified and normalized against the amount of immunoprecipitated Myc-tagged Vps34 as measured by western blot (upper panel). The quantified results (lower panel) show that overexpressing Atg14L significantly upregulated Vps34 kinase activity by 2.5-fold, but only when Beclin

1 was also overexpressed ($*P = 0.04$, one-tailed Student's *t*-test with unequal variances, $n = 5$). **(d)** Colocalization of co-expressed Atg14L-EGFP (green) and Beclin 1-AsRed (red) in punctate structures in transiently transfected HeLa cells. Scale bar, 10 μ m. **(e)** Electron microscopy images show large structures (asterisks) that are often enwrapped with double membranes in the HEK 293T cells co-transfected with Atg14L-EGFP and Beclin 1-AsRed: concentric membrane 'rings' (panel 1); two large structures (3–5 μ m in diameter, panel 2) containing material with high electron density (inset, enwrapping double membranes); numerous autophagosomes (arrows, panel 3) in the cytoplasm; immuno-electron microscopy image of a Atg14L-Beclin 1 structure (labelled with anti-GFP antibody and developed by DAB, panel 4) enwrapped with concentric membrane 'rings'. M, mitochondria; N, nucleus. Scale bar, 500 nm. **(f, g)** EGFP-Atg12 **(f)** or EGFP-Atg5 **(g)** (green) was colocalized with the large structures (arrows) that were labelled by Atg14L-AsRed (red) and Beclin 1-Myc (blue) in transfected HeLa cells. Some of these structures seemed to be 'ring'-shaped (yellow arrows and inset). Scale bar, 10 μ m. See Supplementary Information, Fig. S6 for full scans of blots in **a** and **c**.

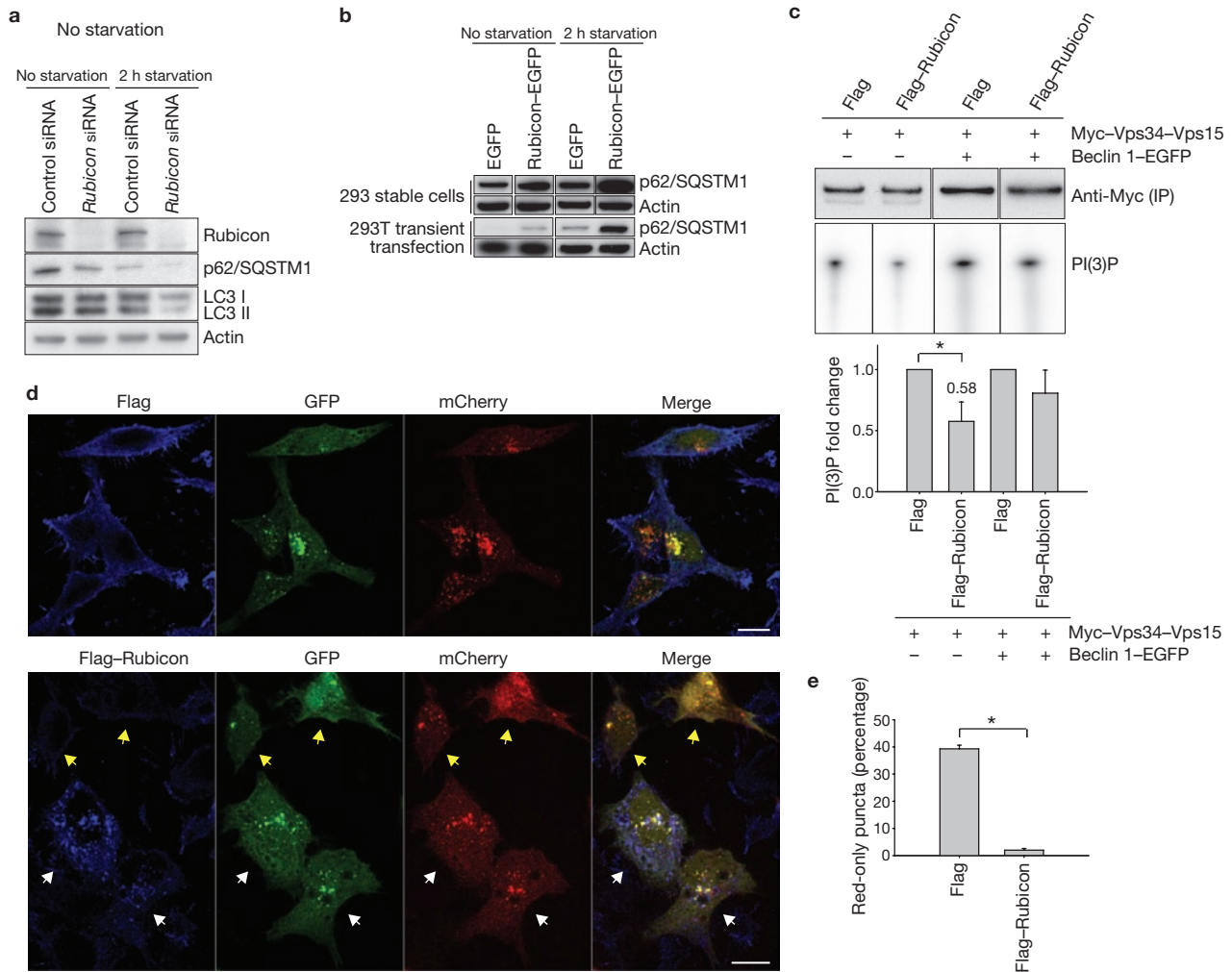


Figure 3 Rubicon is a negative regulator of autophagy. **(a)** *Rubicon* siRNA treatment of the NIH 3T3 cells led to decreased levels of p62 and LC3 II under both normal and nutrient-starvation conditions. **(b)** Overexpression of Rubicon resulted in increased levels of p62 under both normal and nutrient-starved conditions in HEK 293 cells either stably expressing (upper rows) or transiently transfected with (lower rows) Rubicon-EGFP. The control cells were either stably expressing or transiently transfected with the EGFP-N3 vector. **(c)** Vps34 kinase activity. HEK 293T cells were co-transfected with Myc-Vps34-Vps15 and Flag-Rubicon or Flag vector, either in the absence or in the presence of Beclin 1-EGFP. Myc-Vps34-Vps15 was immunoprecipitated by an anti-Myc antibody and used for the *in vitro* kinase assay. The resulting radioactive PI(3)P was separated by TLC, quantified and normalized against the amount of immunoprecipitated Myc-tagged Vps34, as measured by western blotting (upper panel). The quantified results (lower panel) show that overexpressing Rubicon significantly downregulated the Vps34 kinase activity to 0.58-fold, but only without Beclin 1 overexpression ($*P = 0.04$, one-tailed Student's *t*-test with unequal variances, $n = 4$). **(d)** Effect of overexpressing Flag-Rubicon on autophagosome acidification, as

monitored by mCherry-GFP-LC3 fluorescence. HeLa cells were transiently co-transfected with mCherry-GFP-LC3 and Flag-Rubicon (or control Flag vector). Cells co-expressing mCherry-GFP-LC3 and control Flag vector contained many red-only puncta along with yellow (indicating the presence of both red and green) puncta, suggesting the presence of both autolysosomes and nascent autophagosomes (upper panel). In contrast, cells co-expressing mCherry-GFP-LC3 and Flag-Rubicon contained primarily yellow or white puncta, suggesting the presence of only nascent autophagosomes (lower panel, white arrows). Notably, some cells, which were co-transfected with mCherry-GFP-LC3 and Flag-Rubicon but expressed high levels of mCherry-GFP-LC3 and undetectable levels of FLAG-Rubicon, contained many red-only puncta (lower panel, yellow arrows). **(e)** Quantification of the results in **d** show that overexpressing Flag-Rubicon markedly reduced the percentage of red-only puncta (mCherry-LC3) from 39% in the control Flag vector-transfected cells to 2% in the Flag-Rubicon-transfected cells ($*P = 2 \times 10^{-26}$, one-tailed Student's *t*-test with unequal variances, $n = 30$), indicating that overexpression of Rubicon blocks autophagosome acidification or maturation. See Supplementary Information, Fig. S6 for full scans of blots in **a-c**.

Fig. S3j). Interestingly, the RUN or Cys-rich domain of Rubicon seemed to inhibit the binding of Rubicon to Beclin 1 and Vps34 (Supplementary Information, Fig. S3j).

We then characterized the composition of the Beclin 1 complexes. Using anti-Atg14L and anti-Rubicon antibodies, we found that Atg14L co-immunoprecipitated with Vps34 (Fig. S4a) and Beclin 1 (data not shown) but not with Rubicon (Supplementary Information, Fig. S4a). Rubicon co-immunoprecipitated with Vps34 and UVRAG, but not with

Atg14L (Supplementary Information, Fig. S4a). Therefore, Atg14L and Rubicon seem to exist in separate Beclin 1 complexes.

We performed gel filtration experiments with tissue extracts prepared from either wild-type (Fig. 1d) or 'rescued' (Supplementary Information, Fig. S4b) mouse liver. For each sample, eighty fractions of the eluent were collected and analysed by immunoblotting. We found that the endogenous Vps34, Beclin 1 (or Beclin 1-EGFP), Atg14L and Rubicon proteins were primarily co-eluted in fractions 38–45 (Fig. 1d;

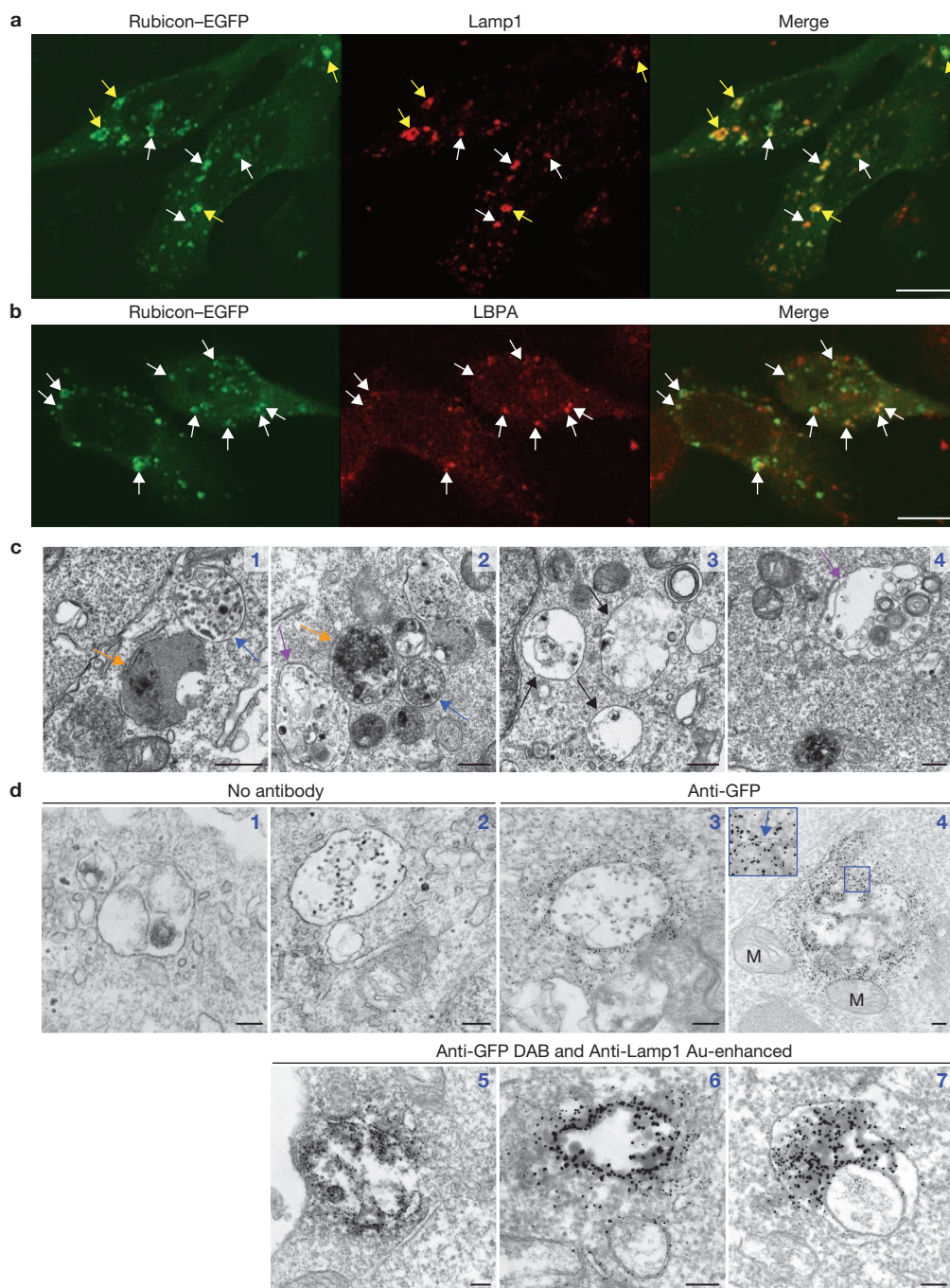


Figure 4 Overexpressing Rubicon causes aberrant expansion of late endosomes/lysosomes. **(a)** Colocalization of Rubicon-EGFP-associated structures with the late endosome/lysosome marker Lamp1 (arrows) in HeLa cells transfected with Rubicon-EGFP. Note that some of the Rubicon-EGFP-associated structures show a 'ring' shape (yellow arrows). Scale bar, 10 μ m. **(b)** Partial colocalization of Rubicon-EGFP-associated structures with the MVB marker LBPA (arrows) in HeLa cells transfected with Rubicon-EGFP. Scale bar, 10 μ m. **(c)** Representative ultrastructural images show aberrant expansion of late endosomal/lysosomal structures in HEK 293T cells overexpressing Rubicon-EGFP. These abnormal organelles are large in

size, with high (orange arrows) or low (black arrows) electron density. Some enclose small vesicles (purple arrows) and some resemble the MVB (blue arrows). Scale bars, 500 nm. **(d)** Representative ultrastructural images show late endosome/lysosome-like structures that are labelled with anti-GFP gold particles (panels 3, 4) in HEK 293T cells transiently transfected with Rubicon-EGFP. These structures are enveloped by double membranes (panel 4 inset) and co-labelled by anti-GFP (developed by DAB) and anti-Lamp1 (gold enhanced) (panels 5–7) antibodies. Note that mitochondria are mostly negative for Rubicon-EGFP (panel 4). The negative controls are without antibody (panels 1–2). M, mitochondria. Scale bars, 200 nm.

Supplementary Information, Fig. S4b), suggesting that these fractions contain a major Beclin 1–Vps34 complex (>700K) that includes both Atg14L and Rubicon. We also performed gel filtration experiments with cell lysates prepared from stable cell lines expressing either Atg14L-EGFP

(Supplementary Information, Fig. S4c) or Rubicon-EGFP (Supplementary Information, Fig. S4d). Again, endogenous Beclin 1 was co-eluted with Atg14L-EGFP (Supplementary Information, Fig. S4c) and Rubicon-EGFP (Supplementary Information, Fig. S4d). Interestingly, starvation of these

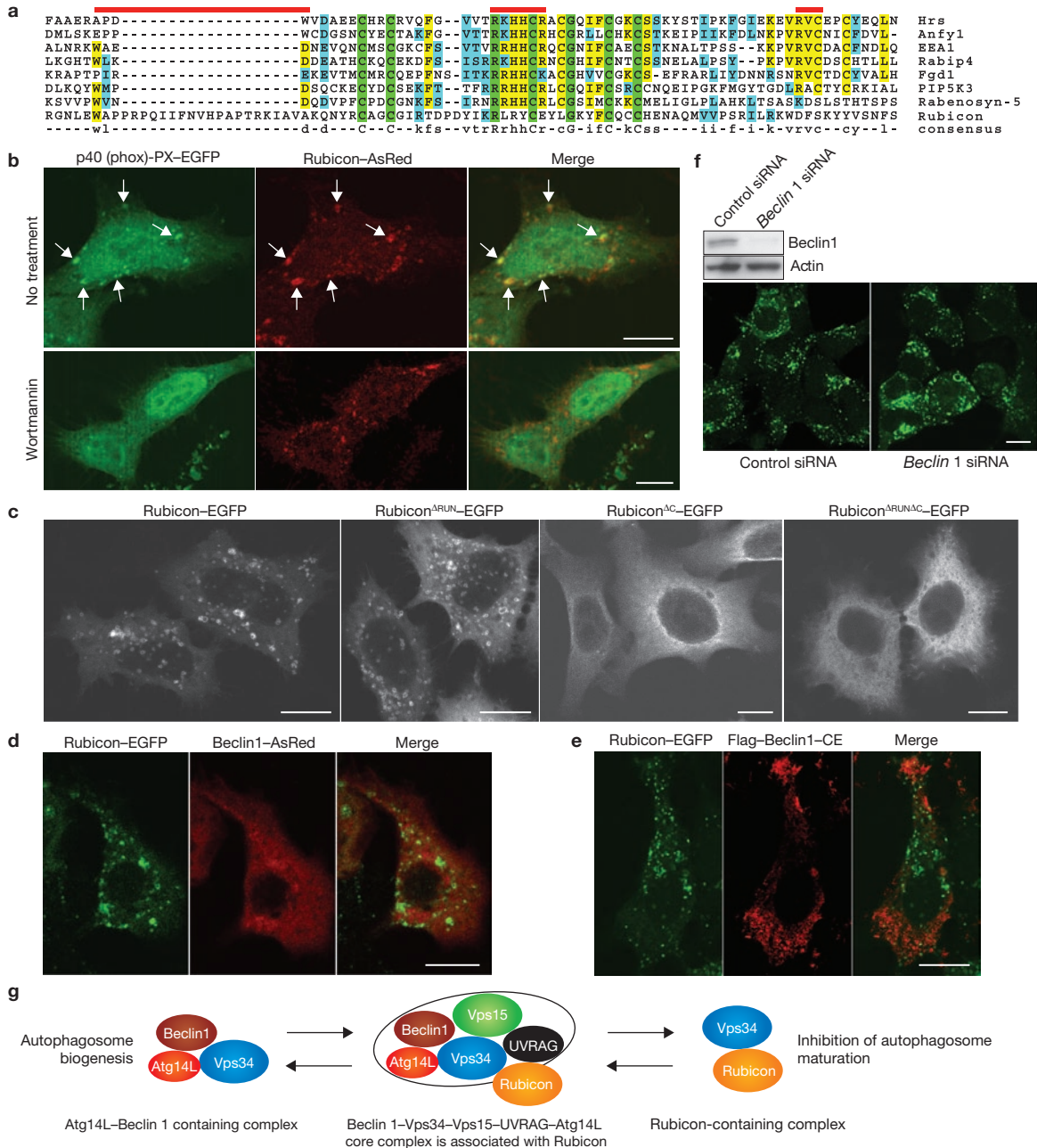


Figure 5 Overexpressed Rubicon is localized on PI(3)P-enriched structures in a Beclin 1-independent manner. **(a)** Local sequence alignment between the C-terminal Cys-rich domain of Rubicon and FYVE domains of several known FYVE-containing proteins. Rubicon does not possess the key consensus sequences of a typical FYVE domain, that is, N-terminal WxxD, central RIR/KIHHCR and C-terminal RVC (indicated by red bars). **(b)** Colocalization of the PI(3)P-enriched lipid domain marker p40 (phox)-PX-EGFP (green) and Rubicon-AsRed (red) on large punctate structures (arrows) in the co-transfected HeLa cells (upper panels). Treatment with the PI(3)K inhibitor wortmannin (75 nM) for 1 h caused disappearance of the PI(3)P-enriched lipid domains, whereas the Rubicon-AsRed-positive structures were maintained (lower panels). Scale bars, 10 μ m. **(c)** Subcellular localization of transiently transfected Rubicon-EGFP, Rubicon^{ΔRUN}-EGFP, Rubicon^{ΔC}-EGFP or Rubicon^{ΔRUNΔC}-EGFP in HeLa cells. In contrast to punctate Rubicon-EGFP and Rubicon^{ΔRUN}-EGFP, Rubicon^{ΔC}-EGFP and Rubicon^{ΔRUNΔC}-EGFP were dispersed in the cytoplasm. ΔRUN, RUN domain deletion; ΔC, cysteine-rich domain deletion. Scale bars, 10 μ m. **(d, e)** Absence of full-length Beclin 1 **(d)** or Beclin 1-CE mutant **(e)** (red) on the Rubicon-EGFP-positive structures (green) in

HEK 293 cells stably expressing Rubicon-EGFP. These cells were transiently transfected with either Beclin 1-AsRed **(d)** or Flag-Beclin 1-CE **(e)**; that is, the Flag-tagged Beclin 1 mutant containing both CCD and ECD, which mediate the Beclin 1-Rubicon interaction as shown in Supplementary Information, Fig. S3h). Scale bars, 10 μ m. **(f)** The formation of the Rubicon-EGFP-positive structures was not affected by siRNA knockdown of *Beclin 1* in HEK 293 cells stably expressing Rubicon-EGFP. **(g)** A model for the Beclin 1-Vps34 protein complexes and their functions. Note that this model is not intended to propose a direct binary interaction. In this model, a core Beclin 1 complex is composed of Vps34/PI(3)K, p150/Vps15, Beclin 1, UVRAG and probably substoichiometric Atg14L (indicated by the tight binding and functional connection between Atg14L and Beclin 1). Under physiological conditions, a large Beclin 1-Vps34 complex is formed, including the core complex and Rubicon. This large complex may be reduced to form smaller complexes, such as an Atg14L-Beclin 1-containing complex and a Rubicon-containing complex. These smaller complexes may be the functional units participating in autophagy regulation through modulating the Vps34 lipid kinase activity. See Supplementary Information, Fig. S6 for full scans of blots in **f**.

stable cells did not affect the elution profiles of Atg14L-EGFP, Rubicon-EGFP and Beclin 1 (Supplementary Information, Fig. S4c–d).

To test the possibility that Atg14L and Rubicon are present in separate protein complexes while co-eluted, we added an anti-Rubicon antibody to the tissue extract before the gel filtration run and immunoblotted the resulting fractions with an anti-Atg14L antibody. Our data show that Atg14L was co-eluted with the anti-Rubicon antibody (Supplementary Information, Fig. S4e), indicating that this antibody binds to the Atg14L-containing complex, suggesting that Rubicon is present in this complex.

Moreover, we observed mutual co-immunoprecipitation of Atg14L and Rubicon from transfected cells, further supporting that Atg14L and Rubicon can be present in the same protein complex (Fig. 1e, f); UVRAG was also co-immunoprecipitated with Atg14L or Rubicon, and the interaction between UVRAG and Rubicon was significantly enhanced in the presence of Beclin 1 (Supplementary Information, Fig. S4f–h).

From these results, we conclude that Atg14L, Rubicon, UVRAG, Beclin 1, p150/Vps15 and Vps34 can form a major Beclin 1–Vps34 complex *in vivo*. However, Atg14L was also eluted in the later fractions (51–56) containing Beclin 1 or Beclin 1–EGFP (but not Rubicon; Fig. 1d; Supplementary Information, Fig. S4b), suggesting that Atg14L is also associated with a smaller Beclin 1 complex without Rubicon.

We performed several assays to determine the role of Atg14L in autophagy. First, we knocked down *Atg14L* expression in cultured cells by RNA interference (RNAi) using a short interfering RNA (siRNA) and analysed the levels of LC3II, a lipid-conjugated form of LC3 that is normally localized on autophagosomes, by immunoblotting^{16–18}. As with *Beclin 1* siRNA, *Atg14L* siRNA resulted in increased levels of LC3II, compared with control siRNA (Fig. 2a, left). Second, we examined levels of p62/SQSTM1, a known autophagy substrate that normally accumulates when autophagy is impaired^{19–21}. Again, like *Beclin 1* siRNA, *Atg14L* siRNA resulted in increased p62/SQSTM1 levels (Fig. 2a). The increase in p62/SQSTM1 and LC3II levels resulting from *Beclin 1* or *Atg14L* siRNA treatment was also significant after starvation (Fig. 2a). Therefore, knockdown of *Atg14L* or *Beclin 1* impaired the autophagy-mediated clearance of p62/SQSTM1 and LC3II.

Third, we knocked down *Atg14L* expression in MLE12 cells that stably expressed GFP–LC3. In control siRNA-treated cells, many small GFP–LC3 puncta were observed, indicating that basal levels of autophagosomes were present (Supplementary Information, Fig. S5a). In contrast, *Atg14L* siRNA transfection resulted in accumulation of large GFP–LC3 puncta (Supplementary Information, Fig. S5a). These large GFP–LC3 puncta were colocalized with p62/SQSTM1 (Supplementary Information, Fig. S5b) and ubiquitin (Supplementary Information, Fig. S5c), indicating that these are ubiquitylated protein inclusions, as previously shown in *Atg5*- or *Atg7*-deficient mouse-tissues^{22,23}. Ultrastructural analysis showed that *Atg14L* siRNA transfection resulted in a reduced number of autophagosomes (data not shown). These analyses suggest that reduced Atg14L expression abolishes autophagosome formation and increases the levels of ubiquitylated proteins.

Fourth, under nutrient-rich conditions, *Atg14L* siRNA treatment caused a slight decrease in the rate of degradation of long-lived proteins (~10%, $P = 0.007$) when compared with control siRNA treatment. However, this rate was markedly reduced upon nutrient withdrawal (~37%, $P = 5 \times 10^{-6}$); this effect of *Atg14L* siRNA was diminished in the presence of 3-methyladenine, an inhibitor of autophagy (Fig. 2b).

Fifth, we investigated whether Atg14L modulates Vps34 kinase activity using a kinase assay that included Vps15/p150 (ref. 24). Our results show that

co-expression of Flag–Atg14L with Myc–Vps34–Vps15 plasmids resulted in an increase in Vps34 activity that was 2.5-fold higher than that caused by co-expression of control Flag with Myc–Vps34–Vps15 plasmids (Fig. 2c). Interestingly, Atg14L-mediated stimulation of Vps34 activity occurred only when co-expressing Beclin 1. This result suggests that overexpression of Atg14L enhances Vps34 activity in a Beclin 1-dependent manner.

Consistent with a previous report for Beclin 1–EGFP transgenic tissues²⁵, we found that Atg14L–EGFP or Beclin 1–EGFP stably expressed in cells was primarily diffuse in the cytoplasm (Supplementary Information, Fig. S5d). However, co-expression of Atg14L–EGFP and Beclin 1–AsRed resulted in their colocalization on punctate structures (Fig. 2d). Electron microscopy analysis of these Atg14L–EGFP and Beclin 1–AsRed co-transfected cells showed many large ‘organelles’ (~3–5 μm ; Fig. 2e). Some of these structures show concentric ‘rings’ with double membranes (Fig. 2e1, asterisks); many are large vacuole-like structures filled with materials of high electron density (Fig. 2e2, asterisks) and enwrapped with double-membranes (Fig. 2e2, insets) that are readily distinguishable from typical aggresomes or protein aggregates (usually not associated with limiting membranes). These structures are positive for Atg14L–EGFP, as shown by immuno-electron microscopy (Fig. 2e4). We also observed an increased in the number of autophagosomes in these transfected cells (Fig. 2e3).

We next studied the nature of these Beclin 1–Atg14L-resident structures. We found that these structures were negative for Golgi (Supplementary Information, Fig. S5e) or ER (Supplementary Information, Fig. S5f) markers. In contrast, they were colocalized with GFP–LC3 (Supplementary Information, Fig. S5g), suggesting that these Beclin 1–Atg14L structures probably recruit LC3. Moreover, they were colocalized with co-expressed EGFP–Atg12 (Fig. 2f) or EGFP–Atg5 (Fig. 2g), suggesting that these Beclin 1–Atg14L structures may be involved in the early steps of autophagosome biosynthesis by recruiting Atg12 and Atg5.

To investigate the role of Rubicon in autophagy, we knocked down endogenous Rubicon protein levels. In contrast to *Atg14L* or *Beclin 1* siRNA, *Rubicon* siRNA caused reduced steady-state levels of LC3II and p62/SQSTM1 under normal or nutrient-starvation conditions (Fig. 3a), suggesting that knockdown of Rubicon promotes autophagic activity. Conversely, in cells stably or transiently transfected with Rubicon–EGFP, the p62/SQSTM1 protein levels were markedly enhanced, compared with those in cells transfected with EGFP (Fig. 3b), suggesting that overexpression of Rubicon inhibits autophagy.

To examine whether Rubicon also modulates Vps34 lipid kinase activity, we performed the lipid kinase assay described above. Our results show that co-expression of Flag–Rubicon with Myc–Vps34–Vps15 markedly reduced Vps34 activity, but only in the absence of Beclin 1–EGFP overexpression (Fig. 3c). This result suggests that overexpression of Rubicon inhibits Vps34 kinase activity and that this effect does not require Beclin 1.

In previous studies, mCherry–GFP–LC3 was used to examine autophagosome maturation, for example, autophagosome acidification following fusion with late endosomes/lysosomes²⁶. We found that cells co-expressing mCherry–GFP–LC3 and Flag–Rubicon contained primarily yellow fluorescent mCherry–GFP–LC3 puncta (immature autophagosomes), whereas cells expressing only mCherry–GFP–LC3 or co-expressing mCherry–GFP–LC3 and control vector Flag contained considerable numbers of red fluorescent mCherry–GFP–LC3 puncta (mature autophagosomes; Fig. 3d, e). This suggests that overexpression of Rubicon may block autophagy by inhibiting autophagosome maturation.

Interestingly, Rubicon-EGFP (or Flag-Rubicon, data not shown) expression showed punctate subcellular localization (Fig. 4a). The Rubicon-EGFP puncta, some of which were 'ring'-shaped, were occasionally labelled with the early endosomal marker EEA1 (Supplementary Information, Fig. S5h) and were primarily colocalized with the late endosomal/lysosomal marker Lamp1 (Fig. 4a). Moreover, some of the Rubicon-EGFP puncta were positively stained with an antibody against lysobisphosphatidic acid (LBPA; Fig. 4b), an unusual eukaryotic lipid found only in the multi-vesicular body (MVB)²⁷, suggesting that some of the Rubicon-EGFP structures may be related to the MVB²⁸. Electron microscopy analysis of Rubicon-EGFP-transfected cells showed many abnormal, large, vacuole-like structures (1–5 µm in diameter; Fig. 4c). Some of these structures contained high electron density molecules (Fig. 4c1–2), characteristic of late endosomes/lysosomes; some had relatively less content with overall low electron density, which may represent enlarged early-stage endosomes (Fig. 4c3). Notably, some seemed to enclose numerous small vesicles of multiple layers (Fig. 4c2, 4), whereas others resembled the MVB²⁸ (Fig. 4c1–2). Through immuno-electron microscopy using anti-GFP gold particles, we observed that these vacuole-like structures in the Rubicon-EGFP-transfected cells were positive for Rubicon-EGFP. Moreover, Rubicon-EGFP was associated with the limiting membranes of these particular structures (Fig. 4d3, 4). Therefore, these structures corresponded to the fluorescent Rubicon-EGFP puncta (Fig. 4a). In addition, our immuno-electron microscopy result confirmed the colocalization of Rubicon-EGFP and Lamp1 at the ultrastructural level (Fig. 4d5–7).

Bioinformatic analysis revealed that the cysteine-rich domain of Rubicon shares sequence homology with the FYVE domain (Fig. 5a), a well-characterized motif specific for phosphatidylinositol-3-phosphate (PI(3)P) binding²⁹. When examined experimentally, Rubicon-EGFP was not pulled down by PI(3)P-conjugated sepharose beads, in contrast to the control PI(3)P-binding protein 2×FYVE-EGFP (data not shown). However, co-expressed Rubicon-AsRed and p40 (phox)-PX-EGFP, another reporter for PI(3)P binding, showed extensive colocalization (Fig. 5b), suggesting that the Rubicon-associated structures are enriched in PI(3)P. Moreover, wortmanin, an inhibitor of Vps34 kinase, effectively dispersed the p40 (phox)-PX-EGFP puncta but not the Rubicon-AsRed structures (Fig. 5b), suggesting that the maintenance of these Rubicon-associated structures does not depend on PI(3)P. Furthermore, through immunofluorescence imaging of Rubicon truncation mutants, we found that the cysteine-rich domain of Rubicon is required for the formation of the Rubicon-positive structures that are enriched in PI(3)P and associated with the aberrant endosomes/lysosomes (Fig. 5c). Finally, we found that Beclin 1-AsRed or Flag-Beclin 1-CE was excluded from Rubicon-EGFP puncta (Fig. 5d, e); *Beclin 1* siRNA did not affect the formation of the Rubicon-EGFP puncta (Fig. 5f). Therefore, the formation of these Rubicon-associated, late endosomal/lysosomal structures are Beclin 1-independent.

In summary, our study has identified Atg14L and Rubicon, two components in the Beclin 1-Vps34 protein complexes, and reveals their distinct roles in regulating autophagy and Vps34 kinase activity. We show that Atg14L and Rubicon may regulate autophagy by modulating Vps34 activity. Our study also suggests the existence of multiple Beclin 1 protein complexes that are engaged in distinct functions in autophagy regulation (Fig. 5g). The significance of these distinct Beclin 1 complexes remains to be fully elucidated. The dynamic change in protein composition between different functional Beclin 1-Vps34 complexes may have a central role in mediating the Beclin 1-Vps34 activity, which governs multiple cellular events, including autophagy.

Note added in proof: a related manuscript by Matsunaga et al. (Nature Cell Biol. 11, doi:10.1038/ncb1846; 2009) is also published in this issue.

METHODS

Reagents, antibodies and microscopy. See Supplementary Information for details.

Mouse genetics. *Becn1-EGFP/+* mice were generated using BAC mouse transgenics³⁰. *Becn1-EGFP/+* transgenic and *Becn1^{-/-}* mice were genetically crossed to generate the 'rescued' mice in which both endogenous *Becn1* alleles are deleted and only *Becn1-EGFP* transgene is expressed. See Supplementary Information for further details.

Affinity purification and mass spectrometry. Affinity purification of Beclin 1 interacting proteins and mass spectrometric identification of these proteins were carried out as described previously¹⁹ with slight modifications. See Supplementary Information for details.

Plasmid constructs and stable cell lines. Total RNA was extracted from postnatal day 12 mouse whole brain using RNeasy mini kit (Qiagen). Full-length cDNA was synthesized with Omniscript RT kit (Qiagen) and used as templates for PCR amplifications with KOD HiFi DNA polymerase (Novagen). *Becn1* was cloned into *EcoRI* and *BamHI* sites of pEGFP-N3 and pAs-Red vectors (Clontech). Atg14L was cloned into *EcoRI* and *BamHI* sites of pEGFP-N3, pAsRed and pCMV-Flag vectors (Sigma). Rubicon was cloned into *HindIII* and *BamHI* sites of pEGFP-N3, pAs-Red and pCMV-Flag2 vectors. UVRAG was cloned into *XhoI* and *BamHI* sites of the pEGFP-N3 vector. Single or combinations of *Becn1* domains were cloned into *EcoRI* and *BamHI* sites of the pCMV-Flag2 vector. Truncated Atg14L mutants were cloned into *EcoRI* and *BamHI* sites of the pEGFP-N3 vector. Truncated Rubicon mutants were cloned into *KpnI* and *BamHI* sites of the pEGFP-N3 vector. EGFP-Atg12 and EGFP-Atg5 constructs were provided by X. Jiang (Sloan-Kettering Memorial Cancer Center, New York, NY). Myc-hVps34-hVps15-V5-His/pVITRO2 plasmid was described previously²⁴. HEK 293 stable cells stably transfected with pEGFP-N3 vector, Beclin 1-EGFP, Atg14L-EGFP or Rubicon-EGFP were generated as described in the Supplementary Information.

Cell culture. Human embryonic kidney (HEK) 293 and 293T, HeLa and NIH 3T3 cells were maintained in Dulbecco's modified Eagle's medium (DMEM) supplemented with 10% fetal bovine serum (FBS) and 1% penicillin-streptomycin (Invitrogen). MLE12 cells were provided by C. Münz (Rockefeller University, New York, NY) and maintained in DMEM/F12 medium (ATCC) supplemented with insulin (0.005 mg ml⁻¹), transferrin (0.01 mg ml⁻¹), sodium selenite (30 nM), hydrocortisone (10 nM), β-estradiol (10 nM), HEPES (10 mM), L-glutamine (2 mM), 2% FBS and 1% penicillin-streptomycin. Transient DNA transfection was performed using a standard calcium phosphate precipitation procedure, FuGene 6 or Lipofectamine 2000 kit, following the manufacturer's protocol (Invitrogen and Roche Diagnostics). Transfection of NIH 3T3 cells and GFP-LC3 MLE12 stable cells with siRNA was performed with a Lipofectamine RNAi MAX kit following the reverse transfection protocol provided by the manufacturer (Invitrogen). The sequences of siRNA are: Beclin 1, CAGUUGGCACAAUCAUA; Atg14L, UUUGCGUUCAGUUCCUCACUGCGC; Rubicon, GCCUUCAGUCAUGCCACA.

In vitro protein immunoprecipitation. DNA plasmids were transfected into HEK 293T cells. For co-immunoprecipitation experiments, two or three plasmids were transfected simultaneously in equal amounts. Cells were lysed in immunoprecipitation lysis buffer (20 mM HEPES, pH 7.4, 1 mM MgCl₂, 0.25 mM CaCl₂, 0.2% Triton X-100, 150 mM NaCl, EDTA-free protease inhibitor cocktail (PIC, 1 tablet per 10 ml), 200 µg ml⁻¹ phenylmethylsulphonyl fluoride (PMSF), 4 µg ml⁻¹ pepstatin and DNase I). For immunoprecipitation with GFP, anti-Atg14L or Rubicon antibodies, dynabeads M-270 E-proxy (Invitrogen) were conjugated with each antibody, and incubated with cell lysates at 4 °C for 2 h. After the beads were washed five times in immunoprecipitation lysis buffer, proteins were eluted by incubating beads in elution buffer (0.5 mM EDTA, pH 8 and 0.5 M NH₃·H₂O) at room temperature for 20 min, frozen in liquid nitrogen and dried in a vacuum speed centrifuge. For Flag-tagged protein immunoprecipitation, anti-Flag M2 affinity resin (Sigma) was used according to the manufacturer's protocol.

Vps34 kinase assay. Vps34 kinase assay was performed as described previously³¹. Myc-hVps34-hVps15-V5-His/pVITRO2 plasmid was transfected into HEK 293T cells in combination with other Flag- or EGFP-tagged plasmids. Cells were

lysed in 1% Nonidet P-40 lysis buffer (20 mM Tris/pH 7.5, 137 mM NaCl, 1 mM MgCl₂, 1 mM CaCl₂, 100 mM NaF, 10 mM sodium pyrophosphate, 100 μM Na₂VO₄, 10% glycerol, 0.35 mg ml⁻¹ PMSF, protease and phosphatase inhibitor cocktails). Immunoprecipitation was performed with anti-Myc affinity gel beads, according to the manufacturer's protocol (Sigma). Beads (associated with purified proteins) were washed three times in lysis buffer, followed by three washes in washing buffer (100 mM Tris-HCl/pH 7.4 and 500 mM LiCl) and two washes in reaction buffer (10 mM Tris-HCl/pH 7.4, 100 mM NaCl and 1 mM EDTA). Beads were resuspended in 60 μl of reaction buffer and MnCl₂ (10 μl of 100 mM) and sonicated phosphatidylinositol (10 μl of 2 μg μl⁻¹) were added. The reaction was started by the addition of ATP (10 μl of 440 μM) containing γ-³²P-ATP (10 μCi), and beads were incubated for 10 min at room temperature. The reaction was terminated by adding HCl (20 μl of 8 M), and the organic phase was extracted with 160 μl chloroform:methanol (1:1). Extracted phospholipid products were resolved by TLC using a coated silica gel and a solvent composed of chloroform:methanol:H₂O:ammonium hydroxide (v/v/v/v, 9:7:1.7:0.3), followed by visualization with Typhoon 9400 Variable Imager (GE Healthcare Biosciences).

Gel filtration. Liver and brain extracts from both *Becn1*^{+/-} and *Becn1*^{-/-};*Becn1*-GFP/+ mice (4 months of age) were prepared as described in the Supplementary Information. Cell extracts were prepared as described previously¹⁹. Tissue and cell extracts were diluted with equal volumes of 2× pull-out buffer (1× containing 20 mM HEPES, pH 7.4, 1 mM MgCl₂, PIC, 100 μg ml⁻¹ PMSF, 2 μg ml⁻¹ pepstatin, 0.2% Triton X-100 and 150 mM NaCl) and incubated for 15 min at 4 °C. The samples were then subject to ultracentrifugation at 100,000g and the resulting supernatants were used for gel filtration experiments. A Superdex 200 HR10/30 column (Pharmacia) was equilibrated with 2-bed volumes of filtered running buffer (1× pull-out buffer without PIC and Triton-X-100). The column was calibrated using Biorad gel filtration calibrant mixtures that are composed of thyroglobulin (670K), γ-globulin (158K), ovalbumin (44K), myoglobin (17K) and vitamin B₁₂ (1,350). A spike of these calibrants (10 μl) was also added to each sample (240 μl) as internal calibrants. Both calibrants and samples were run at a flow rate of 0.2 ml min⁻¹. For each run, 2-bed volumes of running buffer were used to elute the sample and a total of 80 fractions were collected 25–29 min after starting the runs and at a rate of 1 fraction min⁻¹. Two bed volumes of running buffer were used to wash the column at the same flow rate in between two consecutive runs.

Long-lived protein degradation assay. Long-lived protein degradation was assessed as described previously³². In brief, NIH 3T3 cells were transfected with either control or *Atg14L* siRNA and plated in 12-well plates. After 48 h, DMEM was changed to leucine-free medium supplemented with ³H-L-leucine (1 μCi ml⁻¹). After being pulse-labelled for 24 h, cells were washed three times and cultured in DMEM supplemented with excess unlabelled leucine (5 mM) for 16 h to chase out short-lived proteins. Cells were then washed three times and further cultured for 4 h in DMEM, Earle's Balanced salt solution (EBSS), or EBSS supplemented with 10 mM 3-methyladenine, all containing unlabelled leucine (5 mM). Both medium and cell lysates were subject to trichloroacetic acid (TCA) precipitation. Long-lived protein degradation was calculated as the ratio of TCA-soluble medium to TCA-precipitated cell lysate radioactivity.

Statistical analysis. Statistical analyses were carried out as described previously³³.

Note: Supplementary Information is available on the Nature Cell Biology website.

ACKNOWLEDGEMENTS

This work was supported by National Institutes of Health Grants RNS055683A (Z.Y.), RR00862 and RR022220 (B.T.C.) and by the Howard Hughes Medical Institute (N.H.). We thank A. Tolkovsky for GFP-LC3 HeLa cells, C. Münz for GFP-LC3 MLE12 cells, T. Johansen for mCherry-EGFP-LC3 plasmid and X. Jiang for EGFP-Atg12 and EGFP-Atg5 constructs. We thank W. Yang for help with cell culture and generation of stable cells, and H. Shio, E. Sphicas and A. North in the Bio-Imaging Resource Center at The Rockefeller University for help with microscopy.

AUTHOR CONTRIBUTIONS

Z.Y. and Q.J.W. conceived the project. Z.Y. coordinated all efforts in the study; Z.Y., Q.J.W., Y.Z., N.H. and B.T.C. planned the project; Y.Z. and Q.J.W. performed most of the assays; X.L. assisted with p40 (phox)-PX-EGFP localization and Vps34 kinase analyses; Y.Y. and J.M.B. developed the Myc-Vps34-Vps15 constructs and Vps34 kinase assay protocol; Z.Y., Q.J.W. and Y.Z. wrote the paper.

COMPETING FINANCIAL INTERESTS

The authors declare no competing financial interests.

Published online at <http://www.nature.com/naturecellbiology/>
Reprints and permissions information is available online at <http://npg.nature.com/reprintsandpermissions/>

- Liang, X. H. *et al.* Induction of autophagy and inhibition of tumorigenesis by beclin 1. *Nature* **402**, 672–676 (1999).
- Liang, X. H. *et al.* Protection against fatal Sindbis virus encephalitis by beclin, a novel Bcl-2-interacting protein. *J. Virol.* **72**, 8586–8596 (1998).
- Yue, Z., Jin, S., Yang, C., Levine, A. J. & Heintz, N. *Beclin 1*, an autophagy gene essential for early embryonic development, is a haploinsufficient tumor suppressor. *Proc. Natl Acad. Sci. USA* **100**, 15077–15082 (2003).
- Qu, X. *et al.* Promotion of tumorigenesis by heterozygous disruption of the *beclin 1* autophagy gene. *J. Clin. Invest.* **112**, 1809–1820 (2003).
- Edinger, A. L. & Thompson, C. B. Defective autophagy leads to cancer. *Cancer Cell* **4**, 422 (2003).
- Yue, Z. *et al.* A novel protein complex linking the δ2 glutamate receptor and autophagy: implications for neurodegeneration in lurcher mice. *Neuron* **35**, 921–933 (2002).
- Shibata, M. *et al.* Regulation of intracellular accumulation of mutant Huntingtin by Beclin 1. *J. Biol. Chem.* **281**, 14474–14485 (2006).
- Pacheco, C. D., Kunkel, R. & Lieberman, A. P. Autophagy in Niemann-Pick C disease is dependent upon Beclin-1 and responsive to lipid trafficking defects. *Hum. Mol. Genet.* **16**, 1495–1503 (2007).
- Kihara, A., Kabeya, Y., Ohsumi, Y. & Yoshimori, T. Beclin-phosphatidylinositol 3-kinase complex functions at the trans-Golgi network. *EMBO Rep.* **2**, 330–335 (2001).
- Kihara, A., Noda, T., Ishihara, N. & Ohsumi, Y. Two distinct Vps34 phosphatidylinositol 3-kinase complexes function in autophagy and carboxypeptidase Y sorting in *Saccharomyces cerevisiae*. *J. Cell Biol.* **152**, 519–530 (2001).
- Zeng, X., Overmeyer, J. H. & Maltese, W. A. Functional specificity of the mammalian Beclin-Vps34 PI 3-kinase complex in macroautophagy versus endocytosis and lysosomal enzyme trafficking. *J. Cell Sci.* **119**, 259–270 (2006).
- Stack, J. H., DeWald, D. B., Takegawa, K. & Emr, S. D. Vesicle-mediated protein transport: regulatory interactions between the Vps15 protein kinase and the Vps34 PtdIns 3-kinase essential for protein sorting to the vacuole in yeast. *J. Cell Biol.* **129**, 321–334 (1995).
- Liang, C. *et al.* Autophagic and tumour suppressor activity of a novel Beclin1-binding protein UVRAG. *Nature Cell Biol.* **8**, 688–699 (2006).
- Fimia, G. M. *et al.* *Ambra1* regulates autophagy and development of the nervous system. *Nature* **447**, 1121–1125 (2007).
- Takahashi, Y. *et al.* Bif-1 interacts with Beclin 1 through UVRAG and regulates autophagy and tumorigenesis. *Nature Cell Biol.* **9**, 1142–1151 (2007).
- Kabeya, Y. *et al.* LC3, a mammalian homologue of yeast *Atg8p*, is localized in autophagosomal membranes after processing. *EMBO J.* **19**, 5720–5728 (2000).
- Ichimura, Y. *et al.* A ubiquitin-like system mediates protein lipidation. *Nature* **408**, 488–492 (2000).
- Kabeya, Y. *et al.* LC3, GABARAP and GATE16 localize to autophagosomal membrane depending on form-II formation. *J. Cell Sci.* **117**, 2805–2812 (2004).
- Wang, Q. J. *et al.* Induction of autophagy in axonal dystrophy and degeneration. *J. Neurosci.* **26**, 8057–8068 (2006).
- Yue, Z. Regulation of neuronal autophagy in axon: implication of autophagy in axonal function and dysfunction/degeneration. *Autophagy* **3**, 139–141 (2007).
- Komatsu, M. *et al.* Homeostatic levels of p62 control cytoplasmic inclusion body formation in autophagy-deficient mice. *Cell* **131**, 1149–1163 (2007).
- Hara, T. *et al.* Suppression of basal autophagy in neural cells causes neurodegenerative disease in mice. *Nature* **441**, 885–889 (2006).
- Komatsu, M. *et al.* Loss of autophagy in the central nervous system causes neurodegeneration in mice. *Nature* **441**, 880–884 (2006).
- Yan, Y., Flinn, R. J., Wu, H., Schnur, R. S. & Backer, J. M. hVps15 but not calcium/calmodulin is required for the activity and regulation of hVps34 in mammalian cells. *Biochem. J.* **417**, 747–755 (2009).
- Arsov, I. *et al.* BAC-mediated transgenic expression of fluorescent autophagic protein Beclin 1 reveals a role for Beclin 1 in lymphocyte development. *Cell Death Differ.* **15**, 1385–1395 (2008).
- Pankiv, S. *et al.* p62/SQSTM1 binds directly to Atg8/LC3 to facilitate degradation of ubiquitinated protein aggregates by autophagy. *J. Biol. Chem.* **282**, 24131–24145 (2007).
- Kobayashi, T. *et al.* A lipid associated with the antiphospholipid syndrome regulates endosome structure and function. *Nature* **392**, 193–197 (1998).
- Katzmann, D. J., Dorizzi, G. & Emr, S. D. Receptor downregulation and multivesicular-body sorting. *Nature Rev. Mol. Cell Biol.* **3**, 893–905 (2002).
- Stenmark, H., Aasland, R. & Driscoll, P. C. The phosphatidylinositol 3-phosphate-binding FYVE finger. *FEBS Lett.* **513**, 77–84 (2002).
- Gong, S., Yang, X. W., Li, C. & Heintz, N. Highly efficient modification of bacterial artificial chromosomes (BACs) using novel shuttle vectors containing the R6Kgamma origin of replication. *Genome Res.* **12**, 1992–1998 (2002).
- Miled, N. *et al.* Mechanism of two classes of cancer mutations in the phosphoinositide 3-kinase catalytic subunit. *Science* **317**, 239–242 (2007).
- Gronostajski, R. M. & Pardee, A. B. Protein degradation in 3T3 cells and tumorigenic transformed 3T3 cells. *J. Cell Physiol.* **119**, 127–132 (1984).
- Komatsu, M. *et al.* Essential role for autophagy protein *Atg7* in the maintenance of axonal homeostasis and the prevention of axonal degeneration. *Proc. Natl Acad. Sci. USA* **104**, 14489–14494 (2007).

DOI: 10.1038/ncb1854

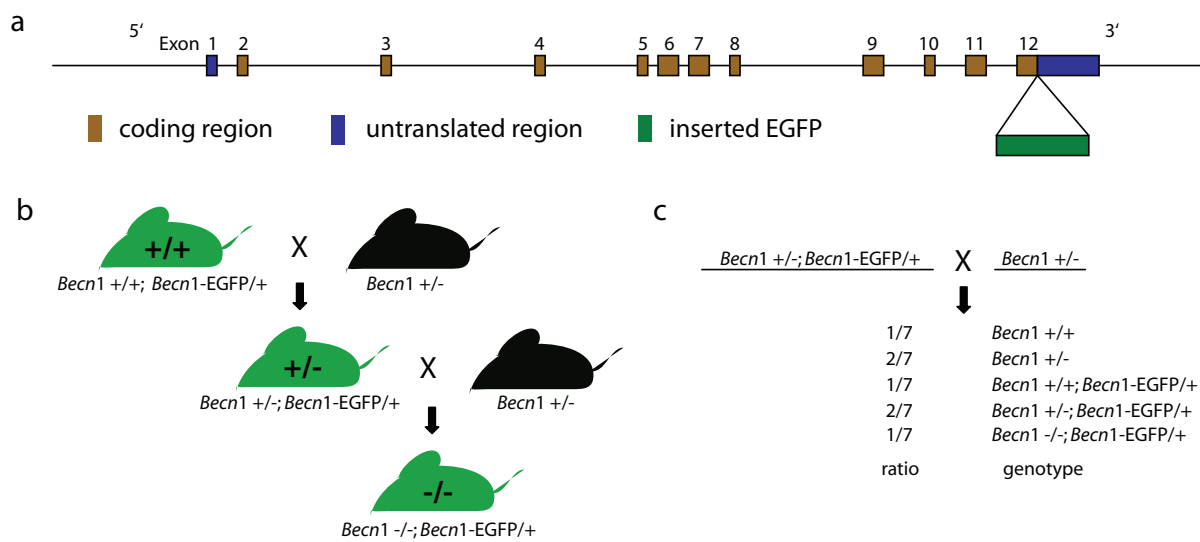


Figure S1 *Becn1-EGFP* transgene rescues the embryonic lethality of *Becn1* homozygous deletion (*Becn1*^{-/-}). (a) Schematic representation of EGFP insertion in BAC-mediated *Becn1-EGFP* transgenics. (b) Breeding strategy for generating mice in which *Becn1-EGFP* transgene replaces the endogenous *Becn1* alleles. *Becn1-EGFP/+* mice were crossed with *Becn1*^{+/-} mice to generate the “rescued” (*Becn1*^{-/-}; *Becn1-EGFP/+*) mice. (c) Theoretical distribution (Mendelian ratio) of each mouse genotype in the

progenies of the indicated breeding pairs. From this breeding, the theoretical fraction of the mouse progenies with the *Becn1*^{-/-}; *Becn1-EGFP/+* is 1/7. In our experiments, eleven out of a total of 69 mouse progenies (from eight litters) derived from the above cross were the *Becn1*^{-/-}; *Becn1-EGFP/+* genotype (*chi* square test with the value 0.22, *p*>0.6, *df*=1), supporting that Beclin 1-EGFP functionally substituted for the endogenous Beclin 1 protein and completely rescued the early embryonic lethality of the *Becn1*^{-/-} mice.

SUPPLEMENTARY INFORMATION

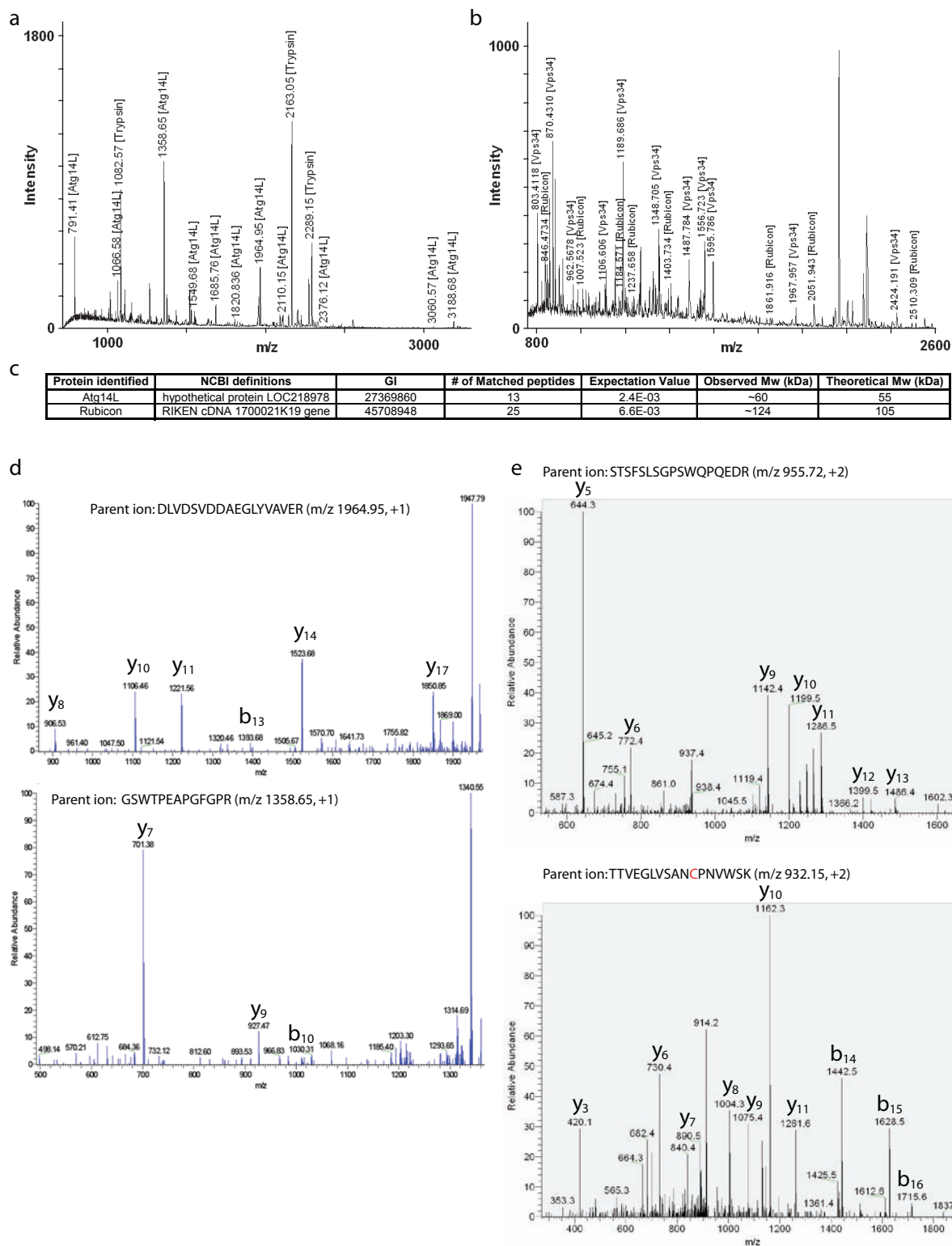


Figure S2 Identification of Atg14L and Rubicon by mass spectrometry. **(a)** Mass spectrum of Atg14L identified from the gel band #6 (Fig. 1b). The sequence coverage was 35.5%. **(b)** Mass spectrum of Rubicon identified from the gel band #2 (Fig. 1b). The sequence coverage was 32.0%. **(c)** Summary of the peptide mapping results for Atg14L and Rubicon. **(d)** Representative tandem mass spectra of two Atg14L tryptic

peptides, as identified by a MALDI ion trap mass spectrometer. **(e)** Representative tandem mass spectra of two Rubicon tryptic peptides, as identified by a LC-MS (ESI linear ion trap) mass spectrometer. The cysteine residue in the second peptide contains a carbamidomethyl modification (in red). This particular sample was isolated from brains of the “rescued” mice starved for 48 h.

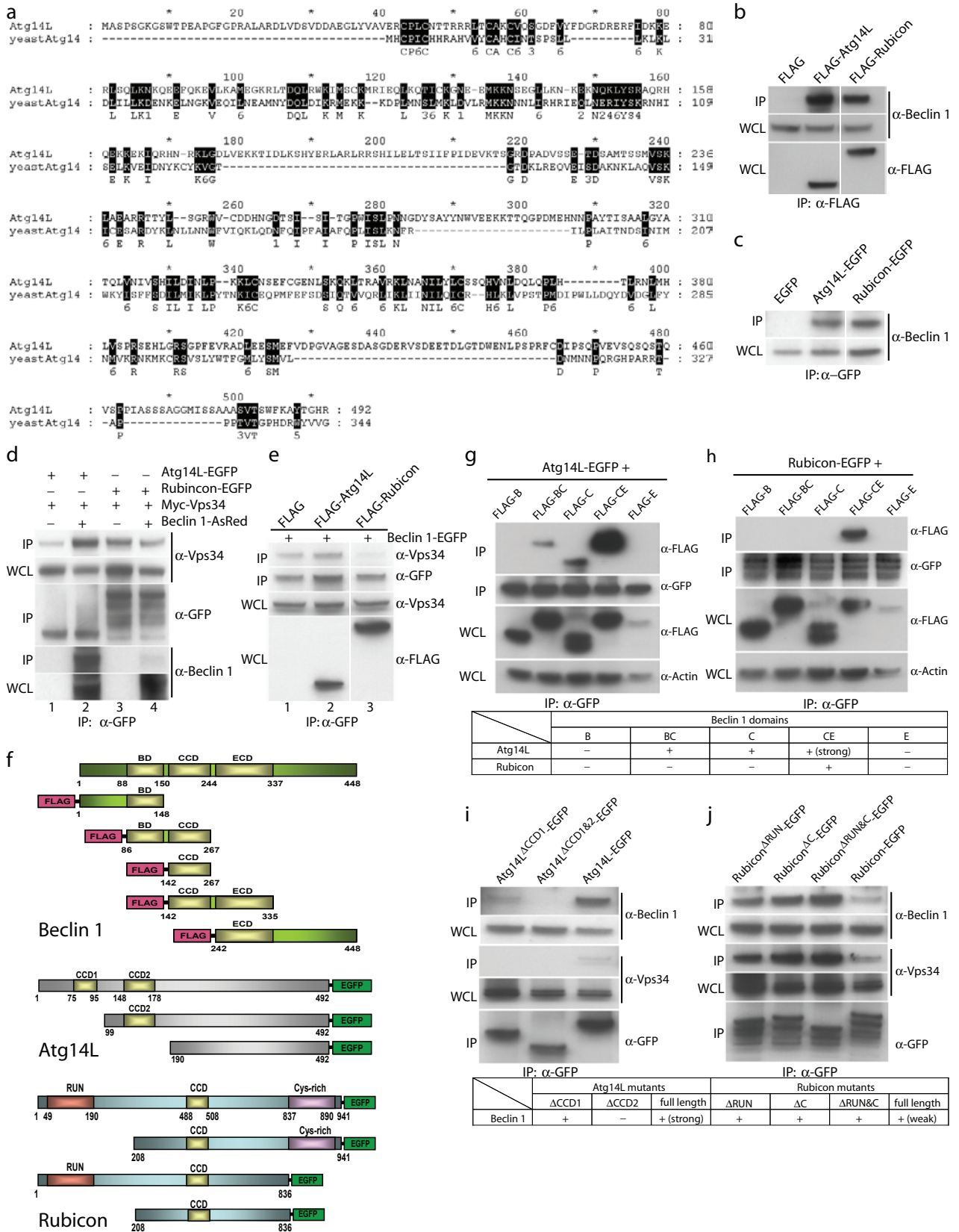


Figure S3 Characterizing the interaction between Beclin 1 and Atg14L or Rubicon. **(a)** Moderate homology between Atg14L and yeast Atg14. Protein sequences of Atg14L and yeast Atg14 were aligned to analyze possible homology between them. Alignment was done using T-Coffee package (Tree based Consistency Objective Function For Alignment Evaluation) (<http://www.tcoffee.org>). The analysis was performed with GeneDoc application. The exact match between Atg14L and yeast Atg14 was 15%, and juxtaposition greater than zero was 27%. The numbers indicate similar groups: 1, DN; 2, EQ; 3, ST; 4, KR; 5, FYW; 6, LIVM. **(b-c)** Confirming Beclin 1-Atg14L and Beclin 1-Rubicon interactions by reciprocal pull outs. HEK 293T cells were transfected with either N-terminal FLAG-tagged **(b)** or C-terminal EGFP-tagged **(c)** Atg14L or Rubicon. Immunoprecipitation was performed with either anti-FLAG **(b)** or anti-GFP antibody **(c)**. The co-immunoprecipitated endogenous Beclin 1 was detected by Western blot using anti-Beclin 1 antibody. **(d)** Co-immunoprecipitation of Beclin 1 and Vps34 with Atg14L-EGFP and Rubicon-EGFP. Atg14L-EGFP or Rubicon-EGFP was co-expressed with myc-Vps34 or with myc-Vps34 and Beclin 1-AsRed in HEK 293T cells. Immunoprecipitation was performed using anti-GFP antibody followed by Western blot with anti-Vps34 and anti-Beclin 1 antibodies. Notably, Beclin 1/Beclin 1-AsRed that was co-immunoprecipitated by Rubicon-EGFP was considerably less than that was co-immunoprecipitated by Atg14L-EGFP. **(e)** Co-immunoprecipitation of endogenous Vps34 with Beclin 1-EGFP in the presence of over-expressed FLAG-Atg14L or FLAG-Rubicon. Beclin 1-EGFP was co-expressed with FLAG-Atg14L, FLAG-Rubicon or control FLAG vector in HEK 293T cells. Immunoprecipitation was performed with anti-GFP antibody, followed by Western blot with anti-Vps34 antibody to detect endogenous Vps34. Notably, over-expression of FLAG-Rubicon, but not FLAG-Atg14L, repressed the amount of endogenous Vps34 that interacted with Beclin 1-EGFP. **(f)** Schematic representations of Beclin 1, Atg14L and Rubicon domain

structures and the construction of multiple deletion mutants. The Beclin 1 mutants were tagged with FLAG at N-termini. The Atg14L or Rubicon mutants were tagged with EGFP at C-termini. **(g-h)** Mapping Beclin 1 sequence domains that were required for binding to Atg14L or Rubicon. HEK 293T cells were co-transfected with FLAG-tagged Beclin 1 mutant constructs and EGFP-tagged full-length Atg14L **(g)** or Rubicon **(h)**. The immunoprecipitation was performed with anti-GFP antibody, followed by Western blot with anti-FLAG antibody. The results of these experiments are summarized in a table at bottom of panels g and h. "+" or "-" indicated positive or negative interactions between the tested protein domains. These experiments showed that the coiled-coil and evolutionarily conserved domains of Beclin 1 (FLAG-CE) synergistically bound to Atg14L; only FLAG-CE of Beclin 1, not other Beclin 1 mutants, bound to Rubicon. Abbreviations: B – Bcl2-binding domain, C – Coiled-coil domain, and E – evolutionarily conserved domain. **(i-j)** Mapping Atg14L and Rubicon sequence domains that were required for binding to Beclin 1. HEK 293T cells were transfected with EGFP-tagged Atg14L **(i)** or Rubicon **(j)** mutant constructs. The immunoprecipitation was performed with anti-GFP antibody, followed by Western blot of endogenous Beclin 1 with anti-Beclin 1 antibody. The results of these experiments are summarized in a table at bottom of panels i and j. "+" or "-" indicated positive or negative interactions between the tested protein domains. These experiments showed that both CCD1 and CCD2 of Atg14L were important for the binding of Atg14L to Beclin 1, and that the RUN or Cys-rich domain of Rubicon was not required for the binding of Rubicon to Beclin 1. Thus, the central region containing CCD in Rubicon was important for its binding to Beclin 1. Notably, the Rubicon mutants lacking RUN, Cys-rich domain or both had increased binding to Beclin1. Abbreviations: RUN – RUN domain, Cys – cysteine-rich domain. For all Western blots in Figure S3, WCL – whole cell lysate, IP – immunoprecipitated sample.

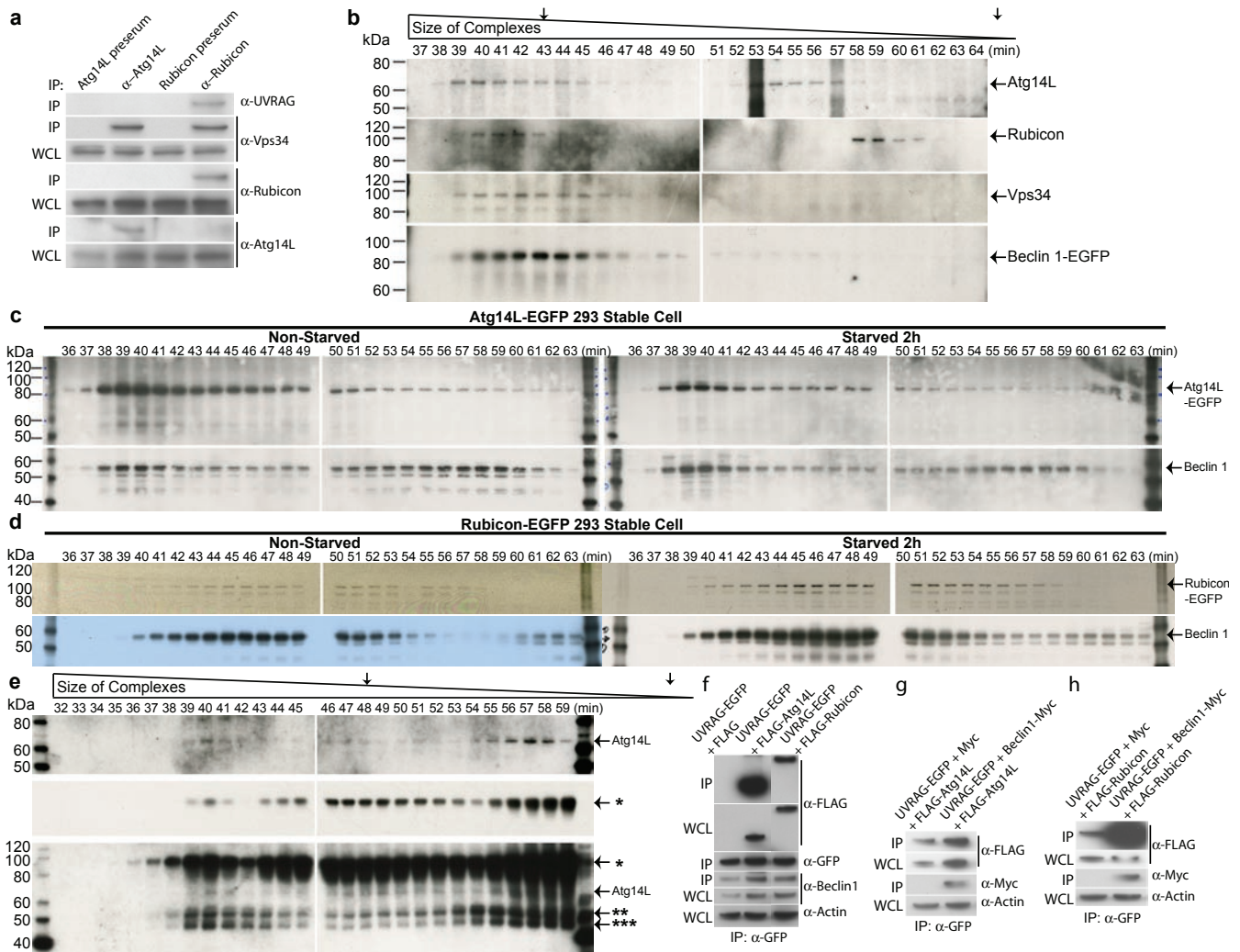


Figure S4 Characterizing the Beclin 1 complexes. (a) Protein-protein interactions between endogenous UVRAG, Atg14L and Rubicon. Immunoprecipitation of endogenous Atg14L- and Rubicon-interacting proteins using anti-Atg14L and anti-Rubicon antibodies from NIH 3T3 cell lysate showed that Atg14L interacts with Vps34 and Rubicon interacts with Vps34 and UVRAG. The control experiments were performed using the corresponding pre-immune sera. The whole cell lysates (WCL) and immunoprecipitated samples (IP) were examined by Western blot with antibodies against UVRAG, Vps34, Atg14L and Rubicon. (b) Western blot analysis of Atg14L, Rubicon, Vps34 and Beclin 1 in the gel filtration fractions from the “rescued” mice liver extract showed co-elution of these proteins in the same fractions 38-45. Atg14L was also eluted in later fractions 51-56. This result is consistent with the observation using wild-type mice (Fig. 1c). The fractions for the peak elution of thyroglobulin (670 kDa) and γ -globulin (158 kDa) are labeled by arrows. (c) Western blot analysis of Atg14L-EGFP and Beclin 1 in the gel filtration fractions of non-starved (left panel) and starved (for 2h, right panel) using Atg14L-EGFP HEK 293 stable cell lysate. Atg14L-EGFP (recognized by anti-GFP antibody as a ca. 85 kDa band) and Beclin 1 co-eluted in the same fractions peaked at 39-40, supporting the specificity of the anti-Atg14L antibody (Figs. 1d & S4b). No change in the elution fractions was detected after the cells were starved for 2h. (d) Western blot analysis of Rubicon-EGFP and Beclin 1 in the gel filtration fractions of non-starved (left panel) and starved (for 2h, right panel) using Rubicon-EGFP HEK 293 stable cell lysate. Rubicon-EGFP and Beclin 1 co-eluted in the same fractions peaked at 47-49, supporting the specificity of the anti-Rubicon antibody (Figs. 1d & S4b). No change in the elution fractions was detected after the cells were starved for 2h. (e) Gel filtration analysis of Atg14L-Rubicon interaction in the Beclin 1-Vps34 complex. The wild type mouse brain extract

was treated either without (upper panel) or with anti-Rubicon antibody (middle and lower panels) before loading onto the size exclusion column. Western blots using anti-Atg14L antibody showed ~65 kDa bands in the same fractions from both samples. In addition, three major anti-Rubicon antibody bands were also detected by the secondary anti-rabbit antibody (labeled by “*”, “***” and “****”). The co-elution of Atg14L and anti-Rubicon antibody suggested that Atg14L and Rubicon were in the same Beclin 1-Vps34 complex. The fractions for the peak elution of thyroglobulin (670 kDa) and γ -globulin (158 kDa) are labeled by arrows. The lower panel is a film with long exposure for the sample incubated with anti-Rubicon antibody before loading onto the size exclusion column. The middle panel is short exposure for the same blot (lower panel) in order to reveal the unsaturated intensity of the strongest antibody band labeled by “*”. (f) Protein-protein interaction between co-expressed UVRAG and Atg14L/Rubicon. HEK 293T cells were co-transfected with UVRAG-EGFP and control FLAG vector, FLAG-Atg14L or FLAG-Rubicon. Co-immunoprecipitation was performed with anti-GFP antibody, followed by detection with anti-FLAG antibody. The result showed that FLAG-Atg14L or FLAG-Rubicon was co-immunoprecipitated with UVRAG-EGFP. (g-h) Effect of Beclin 1 over-expression on protein-protein interactions between co-expressed UVRAG and Atg14L/Rubicon. UVRAG-EGFP was co-expressed with either FLAG-Atg14L (g) or FLAG-Rubicon (h) in HEK 293T cells, in the absence or in the presence of Beclin 1-myc. Co-immunoprecipitation was performed with anti-GFP antibody, followed by detection with anti-FLAG and anti-myc antibodies. The results showed that Beclin 1 over-expression markedly increased the amount of FLAG-Rubicon that was co-immunoprecipitated with UVRAG-EGFP (h) while having little effect on interaction between FLAG-Atg14L and UVRAG-EGFP (g). For (a, f-h), WCL – whole cell lysate, IP – immunoprecipitated.

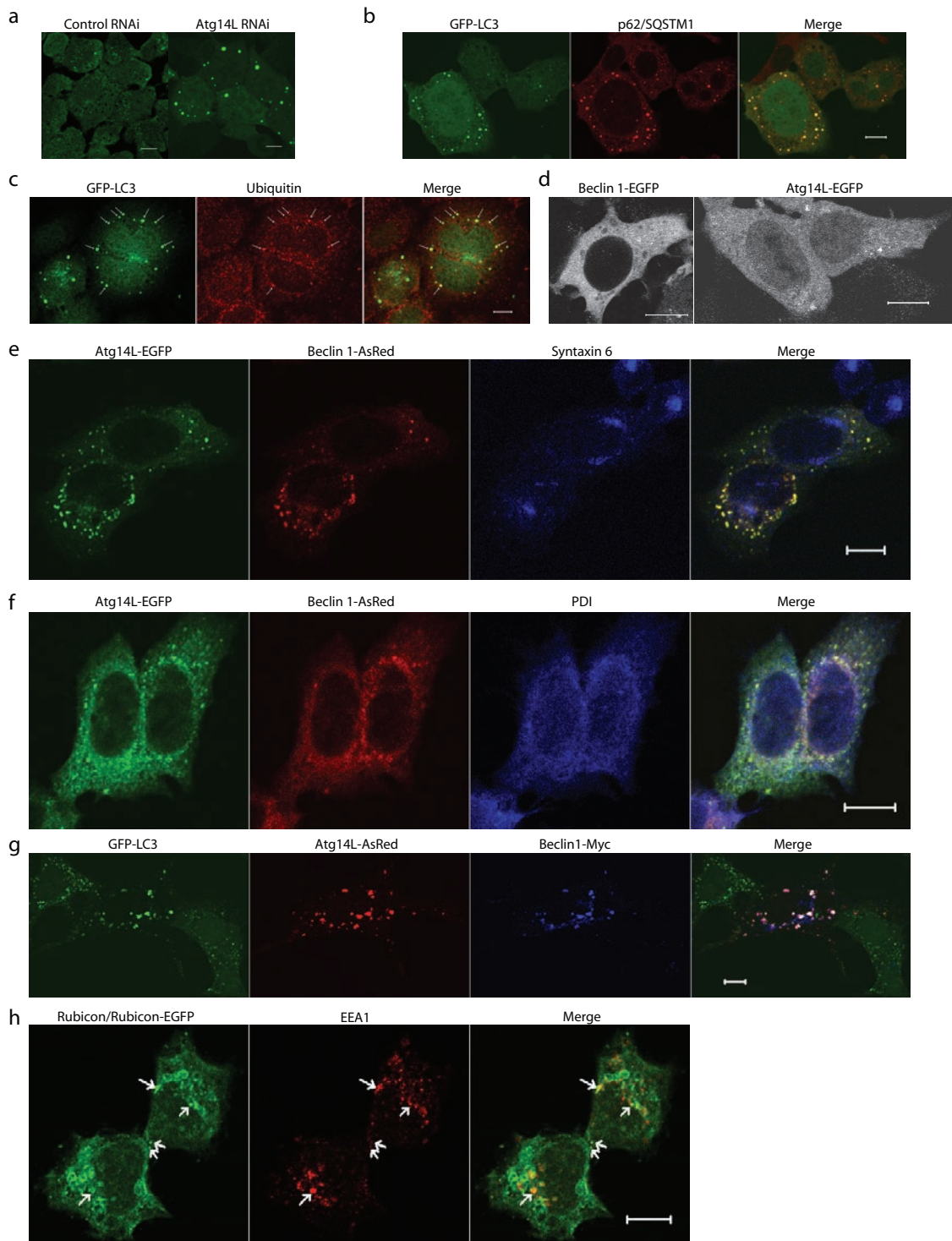


Figure S5 Functional studies of Atg14L and Rubicon. **(a)** Confocal images of MLE12 cells stably expressing GFP-LC3 showed that Atg14L siRNA treatment resulted in markedly increased number of large size GFP-LC3 puncta, as compared to the control siRNA treatment. Scale bars, 10 μm. **(b-c)** Confocal images of MLE12 cells stably expressing GFP-LC3 showed that Atg14L-siRNA-induced large-size GFP-LC3 puncta (green) colocalized with p62/SQSTM1 (b) and ubiquitin (c) (red). Scale bars, 10 μm. **(d)** Beclin 1-EGFP or Atg14L-EGFP was primarily diffuse in cytoplasm of the HEK 293 cells stably transfected with Beclin 1-EGFP or Atg14L-EGFP. Scale bars: 10 μm. **(e-f)** The Atg14L-Beclin 1-positive structures in the HeLa cells transiently transfected with Atg14L-

EGFP (in green) and Beclin 1-AsRed (in red) were not labeled by the Golgi marker syntaxin 6 (e) or the ER marker protein disulphide isomerase (PDI) (f) (in blue). Scale bars, 10 μm. **(g)** Co-localization of Beclin 1-myc (blue), Atg14L-AsRed (red) and GFP-LC3 (green) in the Atg14L-Beclin 1-positive structures in the HeLa cells stably expressing GFP-LC3 and transiently transfected with Beclin 1-myc and Atg14L-AsRed. Scale bar: 10 μm. **(h)** Partial colocalization of Rubicon/Rubicon-EGFP and EEA1 in the HEK 293 cells that were stably expressing Rubicon-EGFP and immunostained with the antibody against Rubicon (pseudocolored in green, actual experiment was performed with Alexa Fluor 555) and EEA1 (pseudocolored in red). Scale bar, 10 μm.

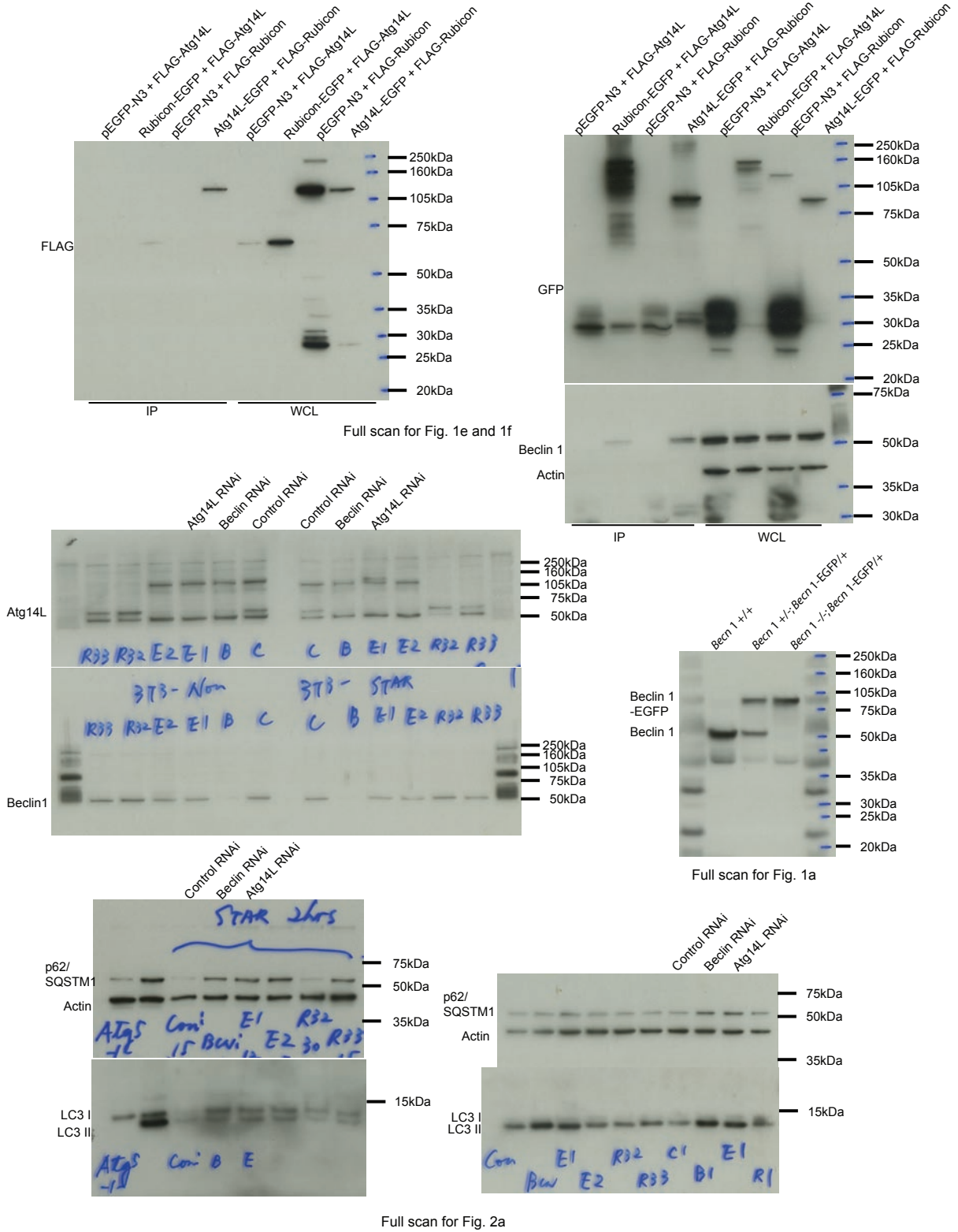


Figure S6 All whole gel images reported in this study.

SUPPLEMENTARY INFORMATION

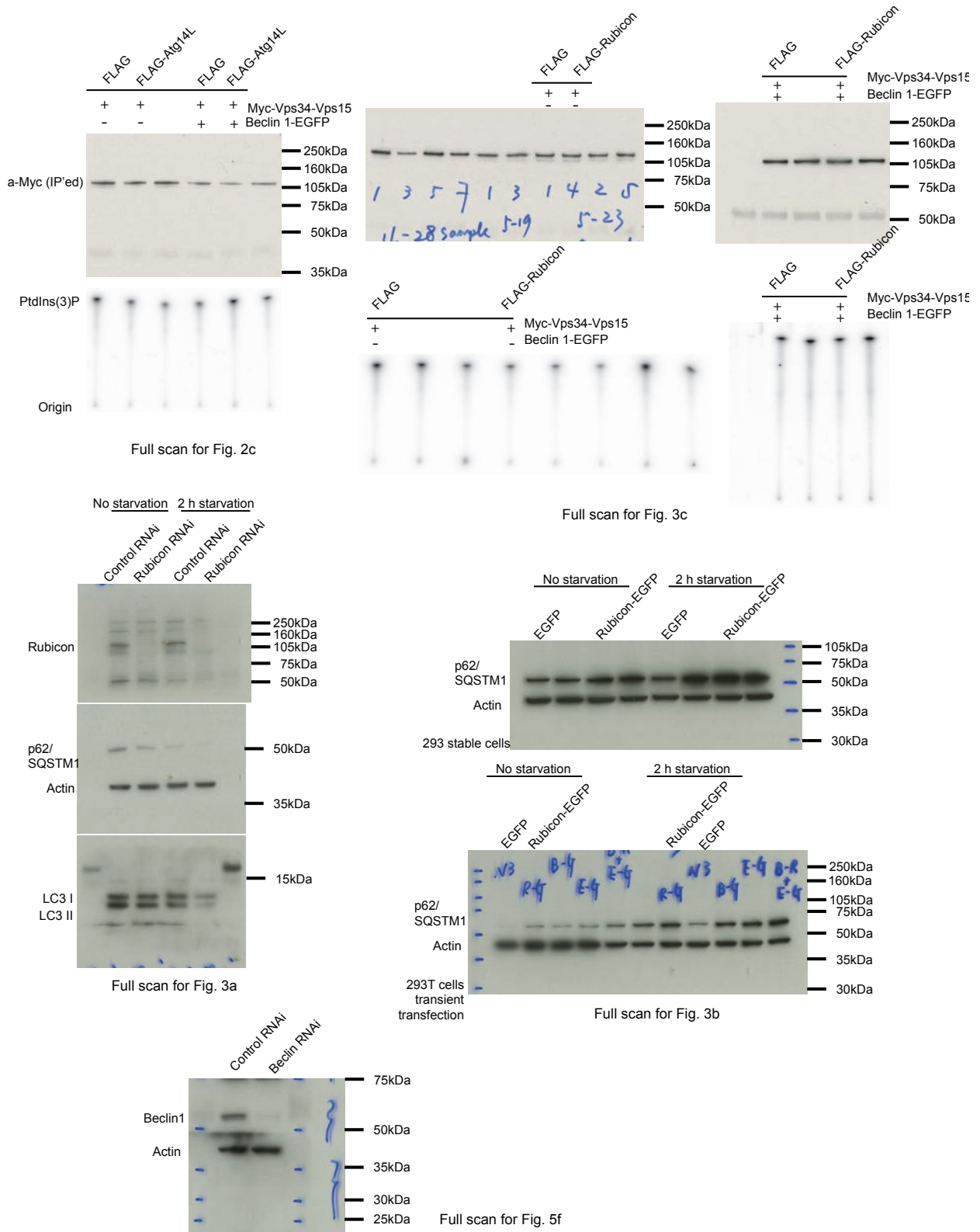


Figure S6 continued

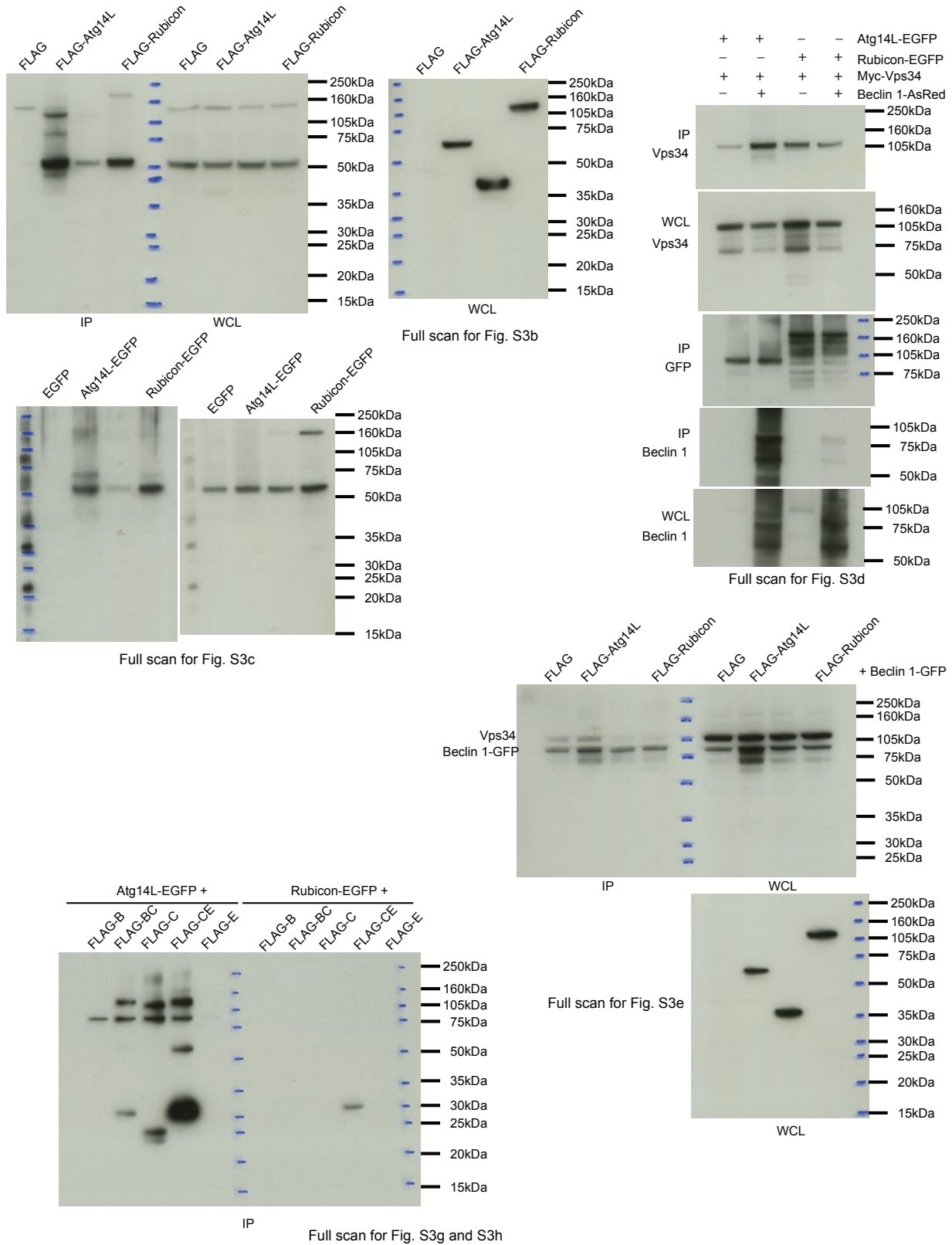


Figure S6 continued

SUPPLEMENTARY INFORMATION

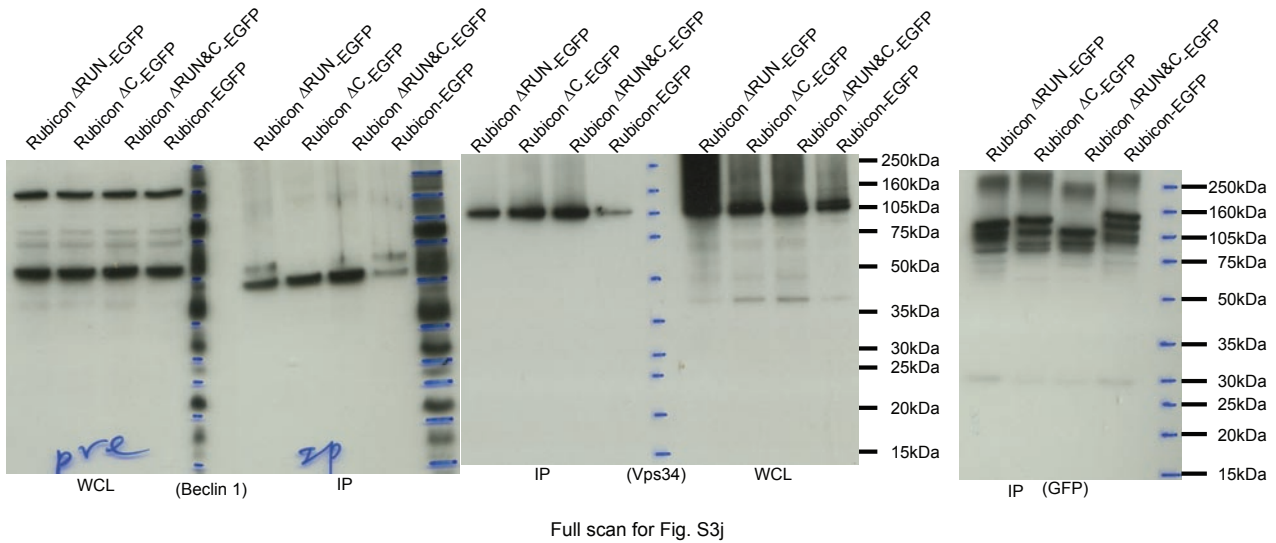
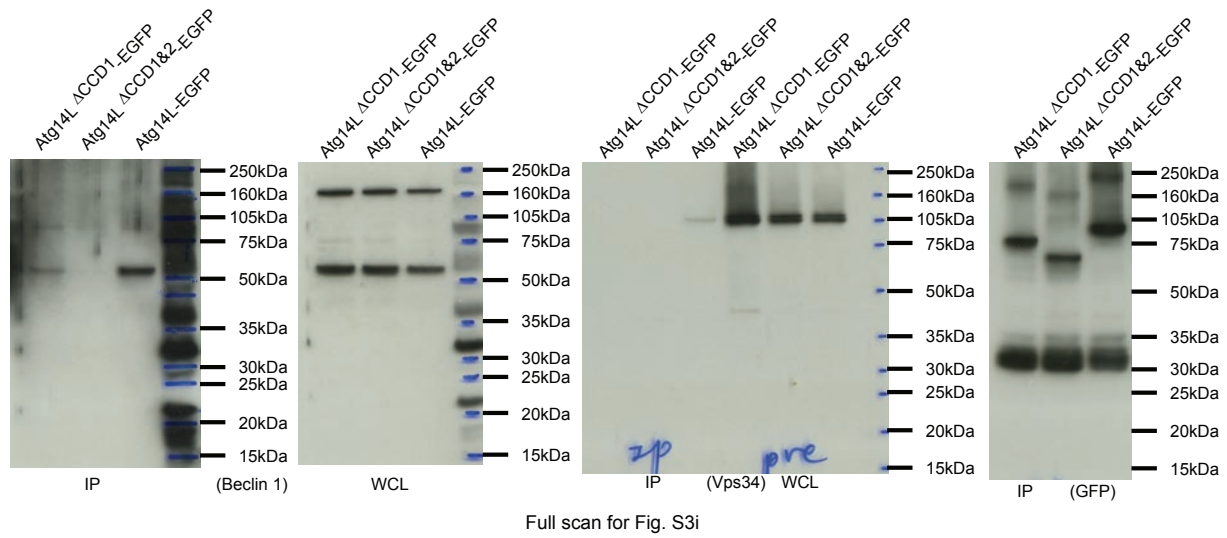
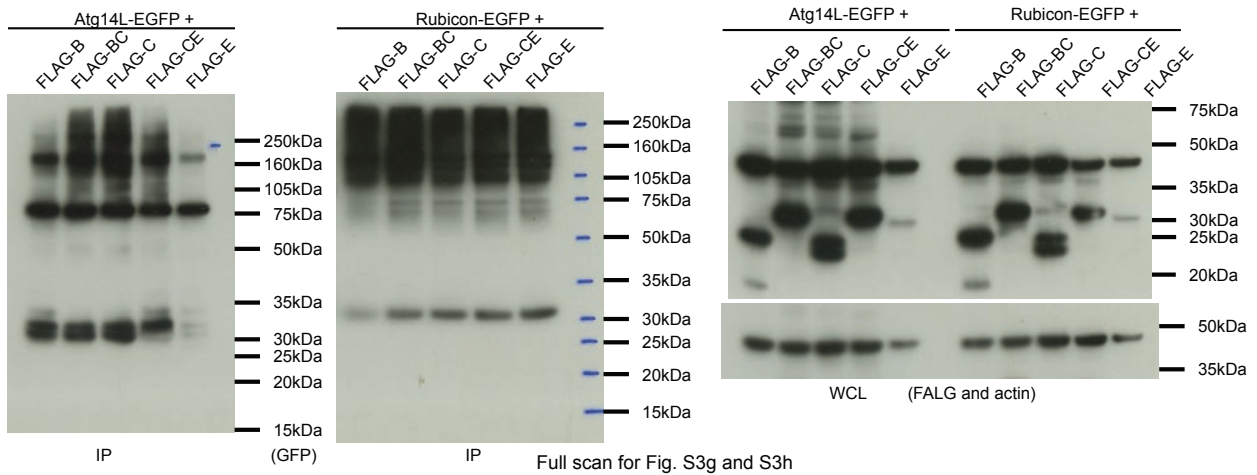


Figure S6 continued

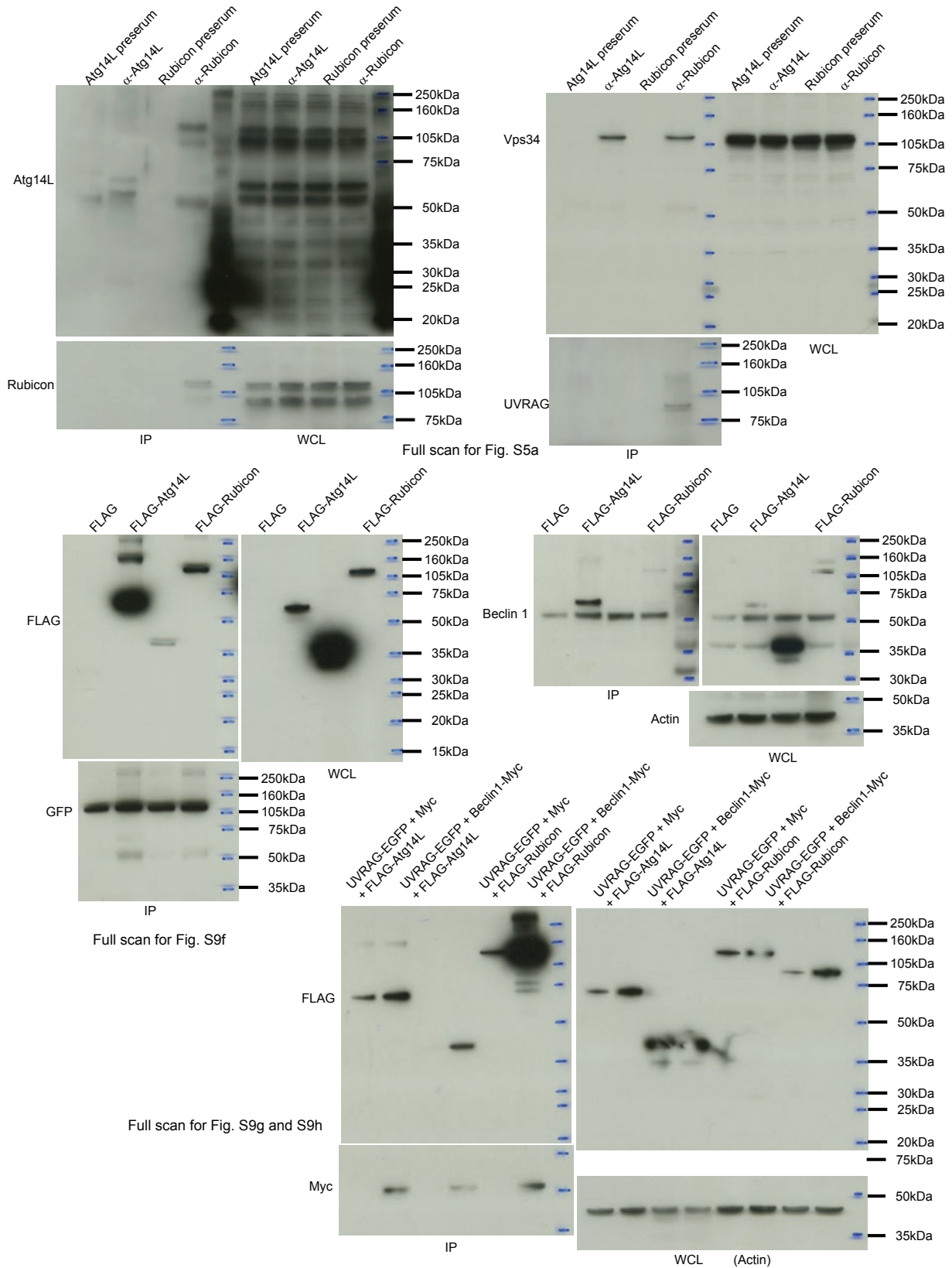
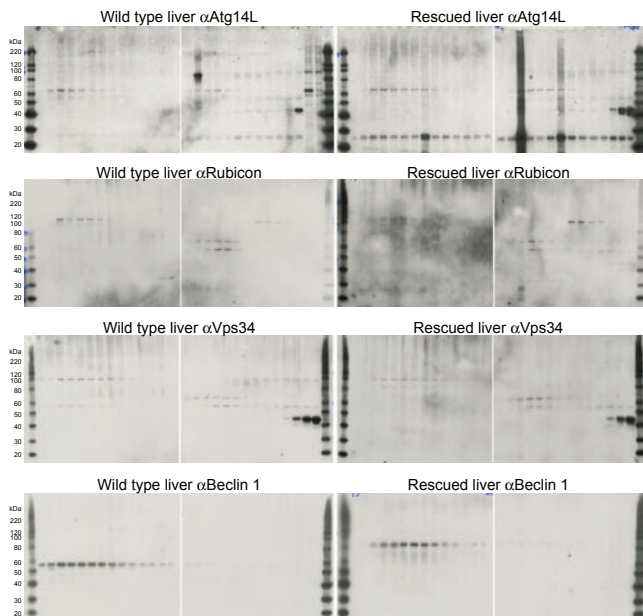


Figure S6 continued

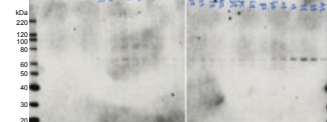
SUPPLEMENTARY INFORMATION

Full scan for Fig. 1d and S4b



Full scan for Fig. S4e

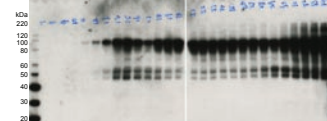
Wild type brain incubated with no antibody prior to gel filtration, αAtg14L



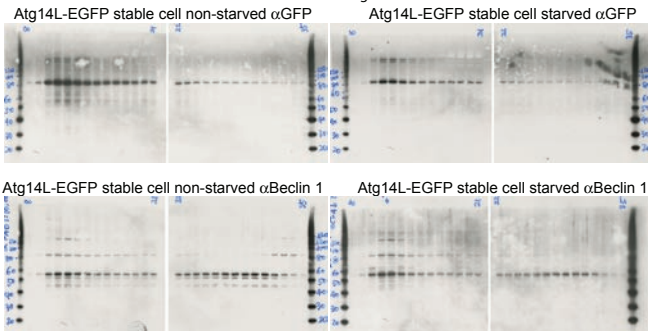
Wild type brain incubated with αRubicon prior to gel filtration, αAtg14L, short exposure



Wild type brain incubated with αRubicon prior to gel filtration, αAtg14L, long exposure



Full scan for Fig. S4c



Full scan for Fig. S4d

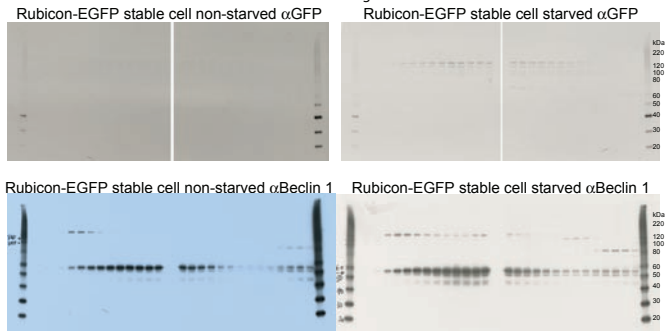


Figure S6 continued

Online Supplemental Information

Supplemental Materials and Methods

Reagents and antibodies

Dynabeads M-270 epoxy, NuPAGE Bis-Tris gels, Western blot transfer buffer, MES SDS running buffer, antioxidant, Lipofectamine 2000 and Lipofectamine RNAi MAX kits were purchased from Invitrogen (Carlsbad, CA). Modified Trypsin, EDTA-free protease inhibitor cocktail tablets, and FuGene 6 transfection reagent were purchased from Roche Diagnostics (Indianapolis, IN). Immobilon-P PVDF membrane was purchased from Millipore (Billerica, MA). GelCode Blue Stain Reagent, Trifluoroacetic acid, Tris(2-carboxyethyl)-phosphine hydrochloride, and the Micro BCA Protein Assay Reagent Kit were purchased from Pierce (Rockford, IL). Gel filtration calibrant mixtures were purchased from BioRad (Hercules, CA). Phosphatidylinositol was purchased from Avanti Polar Lipids (Alabaster, AL). Radio-active ^{32}P -ATP was purchased from PerkinElmer (Waltham, MA). G418, anti-myc affinity gel beads, 3,3'-Diaminobenzidine (DAB) and urea tablets were purchased from Sigma (St Louis, MO). Beclin 1 siRNA was purchased from Dharmacon (Lafayette, CO); Atg14L siRNA was purchased from Invitrogen (Carlsbad, CA); and Rubicon and control siRNA were purchased from Ambion (Austin, TX). Coated silica gel was purchased from EMD (Gibbstown, NJ). Fluorescence mounting medium was purchased from Abcam (Cambridge, MA). Vectastain Elite ABC kit was purchased from Vector Laboratories (Burlingame, CA).

Commercial antibodies used in this study include rabbit polyclonal LC3 antibody (1:1000, MBL, Woburn, MA), rabbit polyclonal antibody raised against the C-terminal of UVRAG (1:500, Abgent, San Diego, CA), rabbit polyclonal Beclin 1 antibody (1:600; Santa Cruz Biotechnology,

Santa Cruz, CA), guinea pig polyclonal p62/SQSTM1 antibody (1:1000, American Research Products, Inc., Belmont, MA), mouse monoclonal Lamp 1 antibody (1:10, Developmental Studies Hybridoma Bank at the University of Iowa, Iowa City, IA), mouse monoclonal LBPA antibody (1:200, Echelon Biosciences Inc. Salt Lake City, UT), rabbit polyclonal Vps34 antibody (1:250, Zymed Laboratories, San Francisco, CA), mouse monoclonal syntaxin 6 antibody (1:600, BD Transduction Laboratories, , San Jose, CA), mouse monoclonal EEA1 antibody (1:600, BD Transduction Laboratories, San Jose, CA), mouse monoclonal protein disulphide isomerase (PDI) antibody (1:100, Abcam, Cambridge, MA), mouse monoclonal c-myc antibody (1:1000; Santa Cruz Biotechnology, Inc., Santa Cruz, CA; Zymed Laboratories, San Francisco, CA), mouse monoclonal M2 FLAG and β -actin antibodies (Sigma, St. Louis, MO), anti-rabbit Alexa Fluo 555 and Alexa 488 (1:1000, Invitrogen, Carlsbad, CA), Rhodamine red conjugated secondary antibody (Jackson ImmunoResearch, West Grove, PA), anti-mouse and anti-rabbit Cy5 (1:500, Zymed Laboratories, San Francisco, CA), rabbit IgG (1:6000; Amersham, Pittsburgh, PA), mouse IgG (1:10000; Pierce, Rockford, IL).

Rabbit polyclonal GFP antibody was raised against GST-tagged GFP and affinity purified in house as described previously¹. Rabbit polyclonal Atg14L and Rubicon antibodies were generated in house as described in the following. Full length cDNA of Atg14L was cloned into NdeI and BamHI sites of bacterial expression vector pET-28a(+) (Novagen, USA). Partial cDNA of Rubicon that corresponds to amino acids 220-941 was cloned into NheI and BamHI sites of pET-28a(+) vector. Recombinant 6 \times His-tagged Atg14L and Rubicon proteins were expressed in BL21-Codon-Plus (DE3)-RIL competent cells and purified with Ni-NTA agarose beads (Qiagen, USA). A total of 500 μ g of purified recombinant protein was used for injections to produce polyclonal antibodies in rabbits (Cocalico Biologicals, Inc. Reamstown, PA). Sera were either

purified with protein-G column (GE Healthcare, Piscataway, NJ) or further affinity purified with recombinant protein.

Generation and genotyping of the *Becn1-EGFP/+* BAC transgenic mice

Becn1-EGFP/+ mice were generated using BAC mouse transgenic techniques². In brief, a 455-base pair homology region immediately upstream of stop codon of *Becn1* gene (“A box”) was PCR amplified and inserted between *AscI* and *SmaI* sites of pLD53.SCA-E-B, and another 507-base pair homology region immediately downstream of stop codon was PCR amplified and inserted between *PacI* and *StuI* sites of the vector (“B box”)². Through homologous recombination, DNA sequence encoding EGFP protein followed by a stop codon was inserted into the BAC clone RP24-392C4 which contains all regulatory elements of *Becn1* gene to replace the original stop codon of *Becn1*. The modified BAC clone was purified using CsCl gradient ultra-centrifugation, and used for pronuclear injection in FVB/NJ mice. All mice were backcrossed to C57BL/6J background for more than 10 generations before analysis.

Genotype of mice from pronuclear injection was determined with either southern blot or PCR reaction. For southern blot, a 0.5-1 inch piece of mouse tail was clipped from the tail end and incubated in lysis buffer (27% sucrose, 1× SSC, 1 mM EDTA, 1% SDS, 200 µg/ml proteinase K) at 55°C overnight. After extractions with phenol:chloroform (1:1) and with chloroform, DNA was precipitated with ethanol and dissolved in TE buffer. Genomic DNA was digested with *XhoI* and *XbaI*, and was analyzed with southern blot using “A box” as the hybridization probe. For PCR reaction, the EGFP forward and reverse primer pairs are: CCTACGGCGTGCAGTGCTTCAGC and CGGCGAGCTGCACGCTGCCGTCCTC.

Generation and genotyping of the “rescued” mice

Becn1-EGFP/+ transgenic mice were genetically crossed with *Becn1*^{+/-} mice to generate the “rescued” mice (Fig. S1b), in which both endogenous *Becn1* alleles are deleted and only *Becn1-EGFP* transgene is expressed. First, *Becn1-EGFP/+* mice were crossed with *Becn1*^{+/-} mice to obtain *Becn1*^{+/-}; *Becn1-EGFP/+* mice. Then mice of this genotype were further crossed with *Becn1*^{+/-} mice to obtain *Becn1*^{-/-}; *Becn1-EGFP/+* mice. Tails were clipped from mice and proteins were extracted in protein lysis buffer (20 mM HEPES/pH7.4, 1 mM MgCl₂, 0.25mM mM CaCl₂, 0.2% triton X-100, 150 mM NaCl, EDTA-free protease inhibitor cocktail (PIC), 200 µg/mL phenylmethylsulfonyl fluoride (PMSF), pepstatin 4 µg/mL and DNase I). Western blot with anti-Beclin 1 antibody was performed to confirm the deletion of endogenous Beclin1 protein. Multiple litters were produced and the numbers of mice of each genotype were counted to examine whether the Mendel’s law was followed.

Affinity purification and mass spectrometric analysis

Affinity purification of Beclin 1 interacting proteins and mass spectrometric identification of these proteins were carried out as described in Wang et al. (2006)³, with slight modification. In brief, tissue extracts were obtained from both *Becn1*^{+/-} and *Becn1*^{-/-}; *Becn1-EGFP/+* mice (4 months of age) by homogenizing 2 brains or 1 liver with a motor-driven homogenizer (speed 2.5, 12 strokes) in 4 ml buffer containing 0.32 M sucrose, 1 mM NaHCO₃, 20 mM HEPES/pH 7.4, 1 mM MgCl₂, 0.25 mM CaCl₂, PIC, 200 µg/mL PMSF, pepstatin 4 µg/mL and DNase I. The tissue extracts were centrifuge at 1,400 g for 10 min and the pellets were homogenized again in 4 ml buffer for 8 strokes and centrifuged again. Supernatants from the two homogenization steps were pooled, centrifuged at 750 g for 10 min. Aliquots of the resulting supernatants were used for gel

filtration experiments. The remaining supernatants were diluted with equal volumes of 2× pull-out buffer and then 2 volumes of 1× pull-out buffer containing 20 mM HEPES/pH 7.4, 1 mM MgCl₂, PIC, 100 μg/mL PMSF, 2 μg/mL pepstatin, 0.2% triton X-100 and 150 mM NaCl. Each sample was incubated with 5 mg M-270 Epoxy Dyanbeads, which were pre-coated with affinity purified polyclonal anti-GFP antibody, for 1.5 hours at 4°C. Dynabeads were washed 5 times with 1× pull-out buffer and then incubated with 250 μl elution buffer containing 0.5 mM EDTA and 0.5 M NH₃·H₂O for 20 min at room temperature. The eluents were collected, frozen in liquid nitrogen and dried in a Speedvac. The purified complexes were resolved on SDS-PAGE and stained with colloidal Coomassie. The entire gel lane of the *Becn1*^{-/-}; *Becn1-EGFP*/+ sample was sliced into ~30 2-mm wide pieces. Each gel piece was reduced, alkylated with iodoacetamide, and subject to in-gel digestion with trypsin. The resulting tryptic peptides were analyzed by MS and MS/MS, using either in-house-constructed MALDI-QqTOF and MALDI-ion trap (LCQ DECA XP; Thermo Electron Corporation) mass spectrometers or ESI-LTQ mass spectrometer (Thermo Electron Corporation). Accurate masses of the tryptic peptides and the masses of their product ions were used to identify proteins in each gel piece, using the computer search engines ProFound (<http://prowl.rockefeller.edu/prowl-cgi/profound.exe>), Xproteo (<http://www.xproteo.com>) and GPM (http://prowl.rockefeller.edu/tandem/the_gpm_tandem.html) to search the most up-to-date NCBI non-redundant mouse protein database.

Generation of stable cell lines

HEK 293 cells were transfected with pEGFP-N3 vector, Beclin 1-EGFP, Atg14L-EGFP or Rubicon-EGFP plasmids, and were selected with 800 μg/ml G418 for one week. Single colonies

with EGFP expression were picked and cultured in medium supplemented with 200µg/ml G418. Correct expression of EGFP-fusion protein was examined with western blot using GFP antibody.

Microscopy

For fluorescence microscopy, cultured cells were fixed in fresh 4% paraformaldehyde in 1× PBS, and permeablized in PBS with either 0.05%-0.1% Triton X-100 or 0.01% saponin for 10-30 min at room temperature. After blocking in PBS containing 10% goat serum for 30 min-1 h at room temperature, cells were incubated in primary antibodies overnight at 4°C. After three washes in PBS, cells were incubated with fluorescent secondary antibodies for one hour at room temperature, followed by four washes in PBS. Cells were mounted with fluorescence mounting medium and examined under Zeiss (Göttingen, Germany) upright or invert confocal microscopes.

For morphology electron miscriscopy (EM), transfected HEK 293T cells were fixed in 2.5% glutaraldehyde (2.5GA) in 0.1M cacodylate buffer/pH 7.4 and processed by routine transmission electron microscopy procedure and embedded in Epon⁴.

For immuno-EM, transfected HEK 293T cells were fixed in fresh PLP fixative (4% paraformaldehyde, 0.01 M periodate, 0.075 M lysine, and 0.075 M phosphate buffer/pH7.4) supplemented with 0.05% glutaraldehyde for 1 h. After three washes in PBS, cells were permeabilized with 0.01% saponin in PBS supplemented with 0.1% BSA for 15 minutes at room temperature, and were incubated with primary antibody (anti-GFP) diluted in the same buffer overnight at 4°C. Vectastain Elite ABC kit was used for secondary antibody incubation, and cells were fixed again in 0.1 M cacodylate buffer supplemented with 1.5% glutaraldehyde and 5% sucrose. After three washes with 50 mM Tris/pH 7.4 supplemented with 7.5% sucrose, DAB

reaction was performed with the same kit. The reaction was stopped with 50 mM Tris/pH 7.4 supplemented with 7.5% sucrose, and cells were processed for enhancement as described⁵.

Blocks were cut with a diamond knife on a Leica UltracutE and ultra-thin (~70 nm) sections were collected on uncoated 200-mesh grids and stained with Uranium and Lead. Grids were viewed with a TecnaiSpiritBT Transmissiion Electron Microscope (FEI) at 80 KV and pictures were taken with Gatan 895 ULTRASCAN Digital Camera.

Image processing

Image levels were processed in Adobe Photoshop (Adobe Systems, San Jose, CA) to enhance contrast.

1. Cristea, I. M., Williams, R., Chait, B. T. & Rout, M. P. Fluorescent proteins as proteomic probes. *Mol Cell Proteomics* 4, 1933-41 (2005).
2. Gong, S., Yang, X. W., Li, C. & Heintz, N. Highly efficient modification of bacterial artificial chromosomes (BACs) using novel shuttle vectors containing the R6Kgamma origin of replication. *Genome Res.* 12, 1992-1998 (2002).
3. Wang, Q. J. et al. Induction of autophagy in axonal dystrophy and degeneration. *J Neurosci* 26, 8057-68 (2006).
4. Yue, Z. et al. A novel protein complex linking the delta 2 glutamate receptor and autophagy: implications for neurodegeneration in lurcher mice. *Neuron* 35, 921-33 (2002).
5. Tecler-Mesbah, R., Wortel, J., Romijn, H. J. & Buijs, R. M. A simple silver-gold intensification procedure for double DAB labeling studies in electron microscopy. *J. Histochem. Cytochem.* 45, 619-622 (1997).